Kaushik *et al. Cell Communication and Signaling* (2025) 23:529
https://doi.org/10.1186/s12964-025-02510-7

Cell Communication and Signaling

RESEARCH Open Access

Temporal transcriptomic profiling reveals distinct age-associated gene expression signatures in gonads under reduced insulin/IGF-1 signaling in *Caenorhabditis elegans*

Neha Kaushik[1], Soumya Rastogi[1], Shivani Kapadia[2,4], Vaibhav Jain[2], Sonia Verma[3], Deepak Pandey[1], Mona Sharma[1], Surabhi Gupta[1], Ashutosh Halder[1], Simon Gregory[2] and Neeraj Kumar[1*]

Abstract

Background Age-related decline in reproductive function is a hallmark of organismal aging, yet the molecular mechanisms driving this process remain incompletely understood. The insulin/IGF-1 signaling (IIS) pathway is highly conserved and influences both lifespan and reproductive aging in *Caenorhabditis elegans*, where reduced IIS extends reproductive span. While prior studies have examined isolated tissues or time points, a comprehensive temporal analysis of gonadal transcriptional dynamics under reduced IIS has been lacking. Here, we compared IIS-dependent regulation of the gonadal transcriptome with that of other somatic tissues to uncover tissue-specific mechanisms of reproductive aging.

Methods Bulk RNA sequencing was performed on distal gonads dissected above the spermatheca from wild-type N2 and *daf-2(e1370)* mutant animals, a well-established model of reduced IIS. Samples were collected at four physiologically relevant adult stages—Day 1 (young adult), Day 2, Day 6, and Day 10—covering early to late reproductive periods. In parallel, whole-worm RNA-seq was conducted for N2 and *daf-2* at Day 1 and Day 10 to enable systemic comparisons. Differential gene expression analyses identified IIS-responsive transcripts that were either gonad-specific or non-gonadal. Expression datasets were further analyzed using self-organizing maps (SOMs) with hierarchical clustering. Gene network construction, functional enrichment, transcription factor enrichment, and conservation analyses were performed, and differential expression profiles were integrated with publicly available germline-, gamete-, and somatic tissue-enriched datasets.

Results Temporal transcriptomic profiling revealed distinct IIS-dependent expression trajectories in gonadal versus non-gonadal datasets. SOM-based clustering resolved temporally regulated expression modules, while network and enrichment analyses uncovered a multilayered regulatory architecture within the gonad. Gonadal expression was enriched for structural, extracellular matrix, and signaling pathway genes, whereas non-gonadal data showed enrichment for stress response and longevity-associated pathways. Integration with germline-, gamete-, and somatic

*Correspondence:
Neeraj Kumar
drnknirwal@aiims.edu

Full list of author information is available at the end of the article

tissue-enriched datasets distinguished tissue-specific regulatory signatures. Importantly, IIS-regulated gonadal components included genes highly conserved with human orthologs.

Conclusion This study provides a high-resolution temporal map of the gonadal transcriptome under reduced IIS and highlights gene modules potentially critical for reproductive maintenance. These findings offer a resource for dissecting tissue-specific aging programs and insulin-dependent regulation of reproductive health.

Plain english summary

As animals age, fertility naturally declines—but the biological reasons behind this are complex. A key player in aging and reproduction is the insulin/IGF-1 signaling (IIS) pathway, which influences how long organisms stay fertile. In this study, we wanted to understand how IIS affects the activity of genes in the reproductive organs over time. To do this, we studied the roundworm *Caenorhabditis elegans*, a common model for aging research. We collected reproductive tissue and whole-body samples from worms with normal and reduced IIS at different stages of adulthood. We then analyzed which genes were turned on or off at each stage. Our results revealed that gene activity changes significantly with age, and that these changes look very different in reproductive tissues compared to the rest of the body. Some genes were found to be tightly regulated by IIS and may help preserve reproductive health as animals age.

This study provides a valuable gene expression map that helps explain how reproductive tissues age under different insulin signaling conditions. It offers a foundation for future research into how to slow reproductive aging through targeted gene regulation.

Keywords Insulin signaling, Gonads, Transcriptomics, Reproductive aging, Caenorhabditis elegans

Background

The aging population and the dramatically rising age of parenthood pose significant medical challenges, leading to a decline in reproductive health and substantial socioeconomic consequences [1, 2]. This decline in female reproductive health, starting approximately one decade before menopause, is attributed mainly to decreased oocyte quality [3]. As maternal age advances, the risks of infertility, miscarriages, and birth defects increase [4]. Aging mammalian oocytes exhibit various abnormalities, such as increased errors in fertilization, chromosome segregation, and cleavage [4, 5]. These issues stem from defects in recombination and chromosome cohesion during meiosis, certain mutations, and a diminished ability to eliminate defective oocytes, which are essential for nurturing developing oocytes [6–9]. Emerging evidence indicates that oocyte quality is not solely determined by germline-intrinsic mechanisms but is also critically shaped by the surrounding somatic gonadal microenvironment [10, 11]. Despite these insights, the molecular impact of aging on the gonad itself remains poorly understood. In this context, *Caenorhabditis elegans* has emerged as a powerful model organism due to its evolutionary conservation with humans in reproductive processes, its transparent anatomy, and its amenability to genetic manipulation. Like humans, *C. elegans* experiences a marked decline in fertility during early to mid-adulthood, offering a tractable system for studying reproductive aging [12]. Understanding how gene expression programs within the gonad change over time, and how they are modulated by conserved aging pathways, is key to unraveling the molecular basis of reproductive longevity.

Insulin/IGF-1 signaling (IIS) is an evolutionarily conserved and potent genetic pathway that regulates reproduction across various organisms, including *Caenorhabditis elegans*, *Drosophila*, mice, and humans [13–19]. In mammals, including humans, the PI3K/AKT pathways downstream of IIS are crucial for recruiting primordial follicles into the growth phase [20]. This process begins when insulin or other growth factors bind to receptors on oocytes and granulosa cells. This binding triggers a downstream cascade that converts PIP2 to PIP3, activating AKT. Activated AKT enhances follicle growth and survival by modulating downstream targets [21, 22]. Granulosa cells and ovarian thecal interstitial cells, both of which are somatic elements, play critical roles in follicle development in humans. Insulin is routinely used to supplement in vitro cultures of preantral follicles, functioning as a survival factor by reducing atresia and increasing the number of viable follicles [23]. IGF1 plays synergistic and complementary roles in granulosa cell development, and insulin can synergize with FSH to promote the differentiation and proliferation of human ovarian interstitial cells [24]. In *C. elegans*, insulin signaling is crucial for germline proliferation, oocyte development, and meiotic progression and for maintaining oocyte quality, thereby influencing reproductive aging [8, 13, 25–27]. Few studies in *C. elegans* have underscored the role of insulin signaling through somatic gonads in maintaining germline progenitor integrity and reproductive fidelity [28, 29]. These observations emphasize that IIS not only regulates germline-intrinsic

processes but also critically influences the surrounding somatic microenvironment to support follicle growth and reproductive success. Although the conserved role of IIS in oogenesis and ovarian development from worms to humans is well established, its temporal and tissue-specific impact on gonadal aging, particularly in the context of advanced maternal age (AMA), remains undefined.

Most existing high-throughput gene expression studies on gonadal tissues have focused on isolated time points, primarily examining either germline-intrinsic programs or gamete-specific processes [30–32]. While informative, such approaches do not capture the dynamic nature of gene regulation in the gonad over the course of reproductive aging. Given that reproductive decline occurs gradually, a temporal framework is essential to uncover stage-specific gene expression signatures, regulatory switches, and coordinated transcriptional programs that contribute to reproductive span. Moreover, the extent to which these programs are shaped by insulin/IGF-1 signaling (IIS)—a central regulator of reproductive and systemic aging—also remains poorly defined. Previous attempts to study tissue-specific gene expression have often relied on gonad-less or germline-ablated *C. elegans* models, which introduce systemic perturbations and compensatory effects that can confound interpretations of native gonadal transcriptional activity. Such genetic interventions can disrupt the organism's interorgan communication network (ICN)—a complex system by which tissues influence each other's physiology—leading to pleiotropic effects and compensatory changes that obscure the native transcriptional landscape [33]. Additionally, these models often carry developmental alterations or systemic shifts unrelated to the intrinsic aging of the gonadal niche, further confounding interpretation. To circumvent these limitations and preserve physiological relevance, we performed high-resolution transcriptomic profiling on manually dissected gonads, carefully excised above the spermatheca to exclude sperm and developing embryos. In parallel, we generated whole-worm transcriptomes to serve as a systemic reference, allowing direct comparisons between tissue-specific and organism-wide gene expression. Using this dual-tissue, temporally resolved approach, we profiled both gonadal and whole-body transcriptomes across physiologically relevant adult stages spanning early to late reproductive periods under wild-type and reduced insulin/IGF-1 signaling (rIIS) conditions. By combining clustering approaches, gene network and functional enrichment analyses, and cross-comparison with tissue-specific datasets, we define distinct IIS-dependent regulatory programs in the gonad. Our results reveal temporal expression modules, uncover a multilayered regulatory architecture, and identify IIS-regulated gonadal components conserved with human orthologs. This analysis revealed distinct, stage-specific gene expression dynamics in the gonad that are not apparent at the whole-organism level. Our strategy enabled the construction of a comprehensive temporal atlas of gonadal gene expression and uncovered how IIS reprograms molecular pathways in the reproductive niche over time.

Methods

Strain maintenance

The *Caenorhabditis elegans* wild-type strain N2 (Bristol) and the *daf-2(e1370)* mutant were procured from the Caenorhabditis Genetics Center (CGC), University of Minnesota, USA. Worms were cultured on nematode growth medium (NGM) agar plates seeded with *Escherichia coli* OP50 as a food source and maintained at 20 °C under standard conditions. Routine subculturing was performed to avoid starvation and overcrowding.

Hypochlorite treatment for egg collection and synchronization of the worm population

Caenorhabditis elegans worms were grown on *E. coli* OP50 bacteria (Caenorhabditis Genetics Centre, Minneapolis, MN, USA) until they reached the egg-containing gravid adult stage. The worms were then collected from the plates via M9 buffer in a 15 mL centrifuge tube. M9 buffer was prepared by mixing 6 g of Na_2HPO_4 (Himedia Laboratories, Mumbai, India, Catalog #TC051), 3 g of KH_2PO_4, 5 g of NaCl, and 0.25 g of $MgSO_4$ in 1 L of double-distilled water. The worms were subsequently centrifuged in a swing bucket rotor (Eppendorf India Pvt. Ltd., Chennai, India, Model #5810R) at 1200 × g for 60 s, followed by resuspension of the worm pellet in M9 buffer. This washing procedure was repeated three times. The worm pellet was then dissolved in a bleach solution composed of double-distilled H_2O, sodium hypochlorite (Merck Life Sciences Pvt. Ltd., Mumbai, India, Catalog #1.00983.0511), and 5 N NaOH (Merck Life Sciences Pvt. Ltd., Mumbai, India, Catalog #1.06462.1000) at a ratio of 7:2:1. To obtain hypochlorite-resistant eggs by dissolving the gravid worm bodies, the suspension was vortexed for 6–8 min using a vortex shaker (Tarsons, Kolkata, India; Model #Spinix). The eggs were then washed 5–6 times by centrifugation at 2000 × g, the M9 buffer was removed with a suction pump (Rocker Scientific Co., Kaohsiung, Taiwan, Model #Rocker410), and the eggs were resuspended in fresh M9 buffer to remove any traces of bleach or alkali. After the final wash, the eggs were resuspended in 10 mL of M9 buffer and kept on a rocking shaker (Tarsons, Kolkata, India, Model #Rockymax) for 18–20 h at 21–22 °C to allow L1 offspring to hatch and arrest. The hatching percentage was assessed to confirm the viability of synchronized L1-stage animals. The L1-arrested worms were then seeded on RNAi plates and grown until the L4 stage. Unhealthy or unsynchronized animals were

discarded at the L4 stage. The remaining healthy and synchronized animals were grown further until they reached the desired stage/time point, at which point they were used for RNA isolation.

Dissection and collection of gonads

Gonads were isolated from *Caenorhabditis elegans* at various time points during the worm lifespan (young adult, day 2, day 6, and day 10), (Table 1). Tools, including a 23 G needle (Generic), Stripper™ pipettor (Cooper Surgical Inc., Trumbull, CT, USA, Catalog #MXL3-STR-CGR), and 75 µm diameter Stripper™ tips (Cooper Surgical Inc., Trumbull, CT, USA, Catalog # MXL3-75), were used. The hermaphrodite worms were transferred to a glass slide placed under a dissection microscope. Using a fine 23 G needle, the worms were carefully severed just behind the pharynx. The extruded gonadal arms were then dissected just above the spermathecae to separate them from the carcass. The isolated gonads were collected with the help of a stripper pipettor in the lid of a 1.5 mL PCR tube containing ice-cold M9 buffer. Five gonads were isolated per tube in a maximum of 10 min. The PCR tubes were capped and spun to bring the gonads down. To each tube, 100 µL of TRIzol containing the gonads was added. The tubes were then rapidly frozen in liquid nitrogen and stored at −80 °C until further analysis.

Whole worm samples were collected from N2 (wild-type) and *daf-2* (rIIS) hermaphrodites at YA (Young-Adult) and Day 10 (Table 1). Approximately 10–15 worms were collected for each technical replicate. To each PCR tube, 500 µl of TRIzol was added. The tubes were promptly frozen in liquid nitrogen and then stored at −80 °C.

RNA isolation

Frozen gonads and worms at −80 °C were lysed via three freeze−thaw cycles with intermittent vortexing to break open worm bodies. To isolate RNA from the gonads, four tubes were prepared, each containing 5 gonads pooled from animals of the same age. 400 µL of chloroform (Merck Life Sciences Pvt. Ltd., Mumbai, India, Catalog #1.07024.0521) was added to the worm pellets, and the tubes were gently inverted several times. After being incubated for 3 min at room temperature, the samples were centrifuged at 12,000 × g for 15 min at 4 °C. The upper aqueous phase was carefully transferred to a fresh tube without disturbing the bottom layer or interphase. An equal volume of isopropanol (Fisher Scientific, Ottawa, ON, Canada, Catalog #BP2618-500) was added, and the mixture was allowed to sit at room temperature for 10 min. Following centrifugation at 12,000 × g for 10 min at 4 °C, the supernatant was discarded, and the remaining pellet was washed with 1 mL of 70% ethanol. After a final centrifugation at 12,000 × g for 5 min at 4 °C, the RNA pellet was air-dried at room temperature and then dissolved in nuclease-free water. The mixture was heated at 65 °C for 10 min with intermittent tapping. The RNA concentration was measured via a fluorimeter (Invitrogen, California, United States, Model #Qubit3.0), and the RNA quality was assessed via a Bioanalyzer with an RNA kit (Agilent Technologies, United States, Catalog #RNA6000Nano).

Table 1 Summary of samples collected for transcriptomic analysis

Sample Type	Strains	D 0 (YA)	D 2	D 6	D 10
Gonads	N2 (Wild-type)	3 BR	3 BR	3 BR	3 BR
	daf-2 (Low IIS)	3 BR	3 BR	3 BR	3 BR
Whole Worm	N2 (Wild-type)	3 BR	X	X	3 BR
	daf-2 (Low IIS)	3 BR	X	X	3 BR

'D' represents days, BR-Biological Replicates and 'X' represents samples not collected

Gene expression analysis via quantitative real-time PCR (q-PCR)

To validate the sequencing results, expression levels of random genes were quantified via real-time quantitative PCR (qRT-PCR). First, complementary DNA (cDNA) was synthesized from 1 µg of total RNA via the SuperScript III First-Strand Synthesis System Kit (Thermo Fisher Scientific, Waltham, MA, United States, Catalog #18080051). The process involved mixing oligo dT primers and dNTPs with the RNA and then heating the mixture at 65 °C for 5 min before cooling it to 4 °C for 1 min. Next, dithiothreitol, RNase OUT, 5x reverse transcriptase buffer, and 1 µL per reaction of Superscript Reverse Transcriptase III were added. The mixture was incubated at 42 °C for 50 min, followed by a termination step at 70 °C for 15 min. Gene quantification was performed via qRT−PCR with Brilliant III Ultra-Fast SYBR QPCR Master Mix (Agilent Technologies, California, United States, Catalog #600882) and a real-time PCR system (Bio-Rad, California, United States, Model #CFX96 Touch Real-Time PCR Detection System) following the manufacturer's instructions. Relative gene expression was calculated via the ΔΔCt method, where the ΔCts values of target genes were normalized to the Ct values of housekeeping gene *gpd-2*. The primers used for this quantitative RT−PCR analysis is listed in Additional File 1.

Library preparation and RNA sequencing

Three biological replicates, each consisting of 20 gonads (4 tubes of 5 gonads each) pooled from animals of the same age and with RNA integrity number (RIN) values above 8, were selected for the study. The cDNA libraries were constructed with a TruSeq RNA Library Prep Kit v2 (Illumina Inc., California, United States) following the manufacturer's instructions. Briefly, 15 ng of RNA sample

was utilized as the starting material. This was followed by mRNA isolation, fragmentation, and priming, followed by first-strand and second-strand cDNA synthesis. The double-stranded cDNA was subsequently purified, followed by adapter ligation and, once again, purification of the ligation reaction. The final step involved PCR enrichment of the adapter-ligated DNA. The quality of the prepared library was assessed via an Agilent 2100 Bioanalyzer, and the quantity was determined via a Bioanalyzer with a high-sensitivity DNA kit (Agilent Technologies, United States, Catalog # 5067 – 4626). Sequencing was then conducted on Illumina next-generation sequencing (NGS) platforms (Illumina Inc., California, United States Models # HiSeq 2500 systems) with 50 bp single-end reads.

Data analysis

Read alignment and differential expression

Standard manufacturer guidelines from Illumina, Inc., were followed for imaging, base calling, and quality scoring. Demultiplexing and conversion of BCL files to FASTQ files were performed via the Illumina-supported CASAVA v1.8.2 software package. MultiQC reports [34] were generated before and after adapter trimming and Phred-based read filtering via Cutadapt to assess data quality. The reads were aligned to the WBcel 245 reference genome with STAR [35], and transcript-level read counts were calculated via FeatureCount [36]. To identify outlier samples and determine factors affecting variation within the expression data, PCAtools (version 2.2) was used for principal component analysis (PCA). Differential expression analysis was performed via DESeq2 [37], and genes with an adjusted P value < 0.05 and $|\log_2 FC| \geq 1$ were considered differentially expressed.

Heatmap generation

Heatmaps were generated via Morpheus online software (https://software.broadinstitute.org/morpheus/) to visual ize RPKM (reads per kilobase of exon model per million mapped reads) values. The data were prepared in tabular format with appropriate headers, uploaded to Morpheus, and visualized via the "Heatmap" tab. Customization options such as clustering, color schemes, and annotations were adjusted for optimal visualization. The resulting heatmaps were saved in PNG format to provide insights into gene expression patterns.

Venn diagrams

Venn diagrams were created via Venny 2.1.0 software, accessible at https://csbg.cnb.csic.es/BioinfoGP/venny.html [38], to depict the overlap among various gene lists. The gene lists were input into the software, which automatically generated Venn diagrams showing common and unique genes across the lists. The results were subsequently manually depicted via MS PowerPoint to illustrate the relationships between the gene sets. The significance of the overlap between different gene lists was evaluated via hypergeometric distribution and representation factors.

Volcano and violin plots

To generate a volcano for gene analysis via the SRPlot tool available at https://www.bioinformatics.com.cn/en?p=2 [39], the gene expression data were prepared in tabular format, ensuring that the columns represented gene identifiers, $\log_2$-fold change values, and p values. Following the website's instructions, the data were uploaded to the SR Plot. The dataset was displayed upon upload, and options were selected to specify columns containing $\log_2$-fold changes and p values for plot generation. Customization settings, including color schemes, point sizes, and labels, were adjusted accordingly. The volcano plot was then analyzed to identify genes exhibiting significant expression changes, with a focus on those with high fold change values and low p values. To ensure fair and biologically meaningful comparisons, only genes that were expressed across all samples were included for violin plot visualization. This approach reduces noise from condition-specific dropout events and stabilizes density estimation across groups. Violin plots were generated using input data where the first column contained gene names and the subsequent columns contained RPKM values for each sample. Various parameters, such as color, size, and shape, were selected from the drop-down menus. Box plots were embedded within each violin plot to illustrate the distribution of the expression data values.

Self-Organizing Map (SOM) analysis

Differentially expressed genes (DEGs), encompassing both upregulated and downregulated transcripts, were identified using the criteria $|\log_2 FC| \geq 1$ and $P \leq 0.05$ across multiple developmental time points: Day 0, Day 2, Day 6, and Day 10 for gonadal tissues, and Day 0 and Day 10 for non-gonadal tissues. Genes showing significant upregulation or downregulation at least at one time point were combined to generate a final non-redundant list for both gonadal and non-gonadal categories. RNA-seq expression data were fetched as reads per kilobase per million mapped reads (RPKM) for gonadal and non-gonadal tissues of *C. elegans* strains N2 (wild type) and *daf-2* mutants at each developmental stage. To capture temporal expression patterns with high resolution, we applied self-organizing map (SOM) analysis. Average RPKM values from three biological replicates were normalized by row-wise Z-score transformation (mean subtraction followed by division by the standard deviation) and further scaled to the range of –1 to 1 by dividing by the maximum absolute value. The SOM architecture

consisted of a 20 × 10 hexagonal grid (200 neurons) with weights initialized from a random normal distribution. Training was performed for 1000 iterations with an exponentially decaying learning rate (initial value = 0.5) and neighborhood radius σ (initial value = 1.0). For each iteration, the best-matching unit (BMU) for each input vector was identified using Euclidean distance. Neuron weights were updated using a Gaussian neighborhood function based on the distance to the BMU. After training, genes were assigned to their nearest neuron according to the minimum Euclidean distance. Visualization was carried out using hexagonal heatmaps for each time point, where neuron colors reflected the average normalized expression of assigned genes. Neurons with no assigned genes were displayed in gray. Expression values were mapped using the 'RdYlBu' colormap (range = − 1 to 1), with black hexagonal outlines (line width = 0.5), equal aspect ratios, and axes removed for clarity.

Hierarchical clustering of expression trajectories

All computational analyses were conducted in Python 3.x using the following libraries: pandas (data manipulation), NumPy (numerical operations), seaborn (color palettes), matplotlib (plotting), scikit-learn (data standardization), and SciPy (hierarchical clustering, linkage analysis, and Pearson correlation calculations). Raw RPKM data were processed by removing duplicate gene identifiers, grouping biological replicates, and calculating mean expression values for each time point: gonadal samples (Days 0, 2, 6, and 10 for N2 and *daf-2*) and non-gonadal samples (Days 0 and 10 for both strains). To stabilize variance and handle zero expression values, data were $\log_2$-transformed with a pseudocount of 1 [$\log_2(\text{RPKM} + 1)$]. Temporal expression patterns were assessed using correlation-based hierarchical clustering to identify genes with similar trajectory shapes, independent of absolute expression levels. Genes with near-zero variance (standard deviation $< 1 \times 10^{-10}$) were removed to prevent computational errors. Pairwise Pearson correlation coefficients were computed on the transposed filtered dataset, and distance matrices were generated as (1 − correlation matrix) to convert similarity into distance measures suitable for clustering. Hierarchical clustering was performed using Ward's minimum variance linkage method. Flat clustering was applied to obtain the predefined number of discrete clusters, with labels assigned sequentially from 0. Genes excluded due to low variance were assigned to cluster − 1, and complete cluster assignment arrays were reconstructed to match the original dataset dimensions. Clustering parameters were optimized separately for each tissue type and strain. For visualization, all gene trajectories were displayed in light gray (α = 0.15) as background, with cluster mean trajectories shown as black dashed lines (line width = 2). For each cluster, a reference gene (highest Pearson correlation to the cluster mean) was identified, and the five genes most strongly correlated with this reference were selected as representative members. These genes were filtered to include only lowercase gene names (characterized genes), sorted by correlation strength, and plotted in distinct colors from the matplotlib 'Table 10' palette (line width = 1.8), with labels indicating gene names and correlation coefficients. Legends were placed at the upper left, with reduced font size (8 pt) and no frame borders.

Transcription factor enrichment

Transcription factor enrichment analysis was conducted via the AnnoMiner tool [40], which leverages promoter regions specific to each transcription factor (TF) on the basis of precalculated binding densities. The analysis was performed on curated, nonredundant gene lists derived from differentially expressed genes in the shared gonadal (ShGn) and non-gonadal (NoGn) categories, as described in the Results section. This tool offers a combined score derived from both the p value and enrichment score, providing a comprehensive assessment of TF enrichment significance. Initially, separate gene lists were prepared for primarily gonadal (ShGn) and Non-gonadal (NoGn) genes exhibiting differential expression. These lists were uploaded to AnoMiner for analysis, with the reference genome set to *C. elegans* (ce11/WBcel245), the genome-annotation resource selected as refseq, and the ID list chosen as nonredundant down (ShGn). The overlap criterion was set to bp overlap with a value of 25 bp, and the promoter region was defined using custom settings specifying 1000 bp upstream and 50 bp downstream from the transcription start site (TSS). Similarly, analysis was performed with other sets of genes. This process yielded a list of enriched transcription factors with their combined enrichment scores. These results were interpreted to identify TFs potentially associated with the regulatory mechanisms underlying the observed gene expression changes. Furthermore, a heatmap based on the enrichment scores was plotted to visualize the TF enrichment patterns.

Network analysis

The gene lists mentioned above with Ensemble ID identifiers were imported to perform network analysis via Cytoscape [41]. The advanced network analysis plugin ClueGO v2.5.8 was used for detailed analysis, pathway enrichment, and representation [42]. The statistical tests used were enrichment/depletion with Bonferroni step-down correction. The GO levels ranged from 3 to 8. The details of the gene cluster samples were included. Manually added or modified IDs, with 3 genes each and a minimum percentage of 4.0. Clusters were combined via 'Or' logic with a specificity threshold of 60.0%. GO fusion was

disabled, while GO grouping was enabled. The kappa score threshold was set to 0.4, and grouping by kappa statistics was enabled, with an initial group size of 1 and a sharing group percentage of 50.0%. Network layout algorithms are applied to organize the network visually. The network is explored interactively, zooming, panning, and selecting nodes and edges to focus on specific regions of interest. The resulting network visualization is customized with labels and annotations for clarity.

Gene ontology (GO) analysis

To perform gene ontology (GO) analysis via the Database for Annotation, Visualization, and Integrated Discovery (DAVID) [43], a list of genes mentioned in the TF enrichment analysis was used. These gene lists were then uploaded to the DAVID website, and the Gene Functional Classification tool was selected from the Analysis Tools menu. After choosing the *C. elegans* species and gene identifier type, the analysis was initiated. DAVID performs functional annotation clustering and GO analysis to identify enriched biological processes, cellular components, and molecular functions within the gene list. The top five categories on the basis of p values are plotted with bar diagrams.

Statistical analysis

Differential expression analysis of the RNA-seq data was conducted via DESeq2 [37]. The raw count data were normalized to size factors, and differential expression was assessed via a negative binomial model. P values were computed via the Wald test and adjusted for multiple testing via the Benjamini–Hochberg procedure to control the false discovery rate (FDR). Genes with an adjusted p value ≤ 0.05 and absolute $\log_2$-fold change ≥ 1 were considered significantly differentially expressed. Hypergeometric p values for all Venn diagrams were computed via online software (http://www.geneprof.org/GeneProf/tools/hypergeometric.jsp), with exact p values reported in the figures. qPCRs were run in triplicate. The fold change in gene expression and relative data was analyzed via an unpaired two-tailed Welch's t test, accounting for unequal variances between the samples. GraphPad version 8.0 (PRISM, San Diego, CA, USA) was utilized for data analysis and graph plotting. Significance was determined at a p value ≤ 0.05. These values are represented as * 0.05, ** 0.01 and *** 0.001.

Results

Gonads exhibit distinct molecular signatures

We selected four distinct time points from N2 (wild-type) and *daf-2 (e1370)*, (Low IIS) worms: young adult (YA) (Day "0", shortly after fertilization begins), Day 2 (peak reproductive period), Day 6 (near the end of the reproductive period in wild-type worms), and Day 10 (as the reproductive period in low-IIS worms nears completion) after growing the worms at 20 °C on OP50 bacterial feed. Whole worm samples were collected at two specific time points: YA on Day "0" and Day 10. The day 2 and day 6 samples from whole worms were excluded from analysis to avoid potential RNA contamination from embryos. After bulk RNA sequencing (Additional File 2), the average RPKM values from three biological replicates for each sample were plotted, revealing a distinct gene expression pattern between the gonads and the whole organism (Fig. 1A). Gene expression levels were markedly higher in the gonads than in the whole organism, although the total number of expressed genes was greater in the whole organism (Additional File 2). To analyze the variability in gene expression, genes were categorized based on their RPKM values. Genes that were expressed in all gonadal samples were identified ($n = 7944$), and a separate set of genes consistently expressed across all whole-worm samples ($n = 13{,}563$) was similarly considered. The Venn diagrams depicting these overlaps are shown irrespective of strain background or sample collection time point. Genes expressed across all samples were categorized based on their expression levels (RPKM) into six groups: Minimal (≤ 1), Low (1–10), Moderate (10–100), High (100–200), Very High (200–500), and Extremely High (> 500). (Additional File 3 and Figure S1A). In the gonads, most genes fell in the Moderate (10–100 RPKM) category across all time points (~ 3800 genes), followed by Low (1–10 RPKM, ~ 1700–1800 genes). Minimal (≤ 1 RPKM), High (100–200 RPKM), Very High (200–500 RPKM), and Extremely High (> 500 RPKM) categories contained fewer genes. Most genes in whole worms were in the Moderate (10–100 RPKM, ~ 5500–6400) and Low (1–10 RPKM ~ 4300–4900) categories. Minimal (≤ 1 RPKM) genes were more abundant than in gonads, while Very High and Extremely High categories contained no genes, suggesting that high-expression transcripts in the gonads are not reflected systemically. The distribution was largely consistent between WT and rIIS whole worms (Figure S1A).

To further elucidate the distribution of gene expression, violin plots combined with kernel density estimates and box plots were generated. These plots revealed that, at the organism level, a substantial proportion of genes had RPKM values below 20, whereas at the gonadal level, a notable fraction of genes presented RPKM values above 20 (Fig. 1B). This suggests a distinct molecular environment in the gonads. Furthermore, nonredundant gene lists for the gonads ($n = 8{,}586$) and the whole organism ($n = 13{,}862$) were curated. The overlap between these gene lists enabled us to categorize genes into two non-overlapping groups: those expressed in both the gonads and the whole organism "Shared Gonadal (ShGn)" and those expressed in the whole organism but not in the

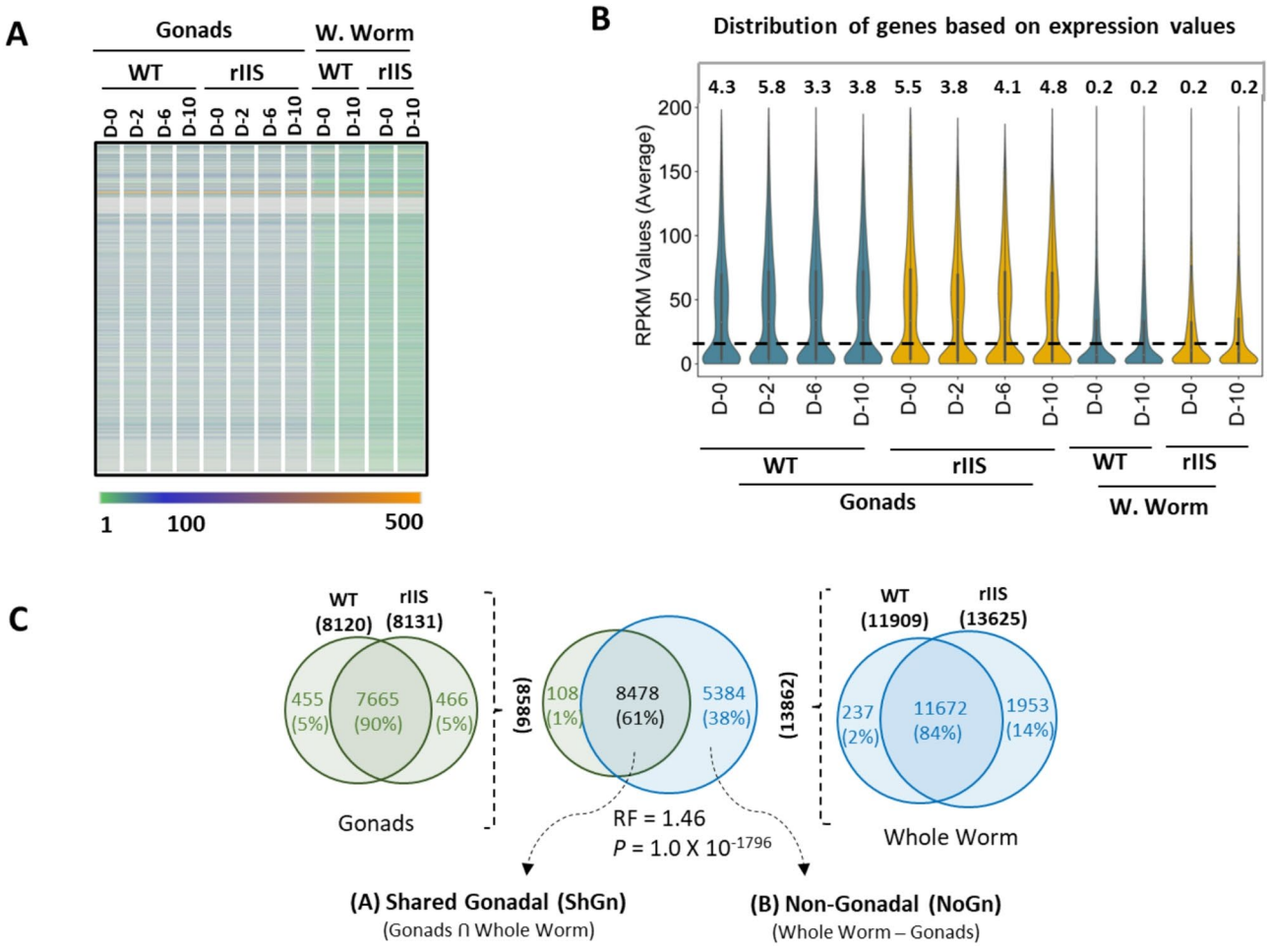

Fig. 1 Comparative transcriptomic profiling of somatic gonad and whole-worm tissue samples. **A** Heatmap depicting cumulative RPKM-based gene expression across three biological replicates ($n = 3$) of gonad samples at Day 0, Day 2, Day 6, and Day 10, and whole-worm samples at Day 0 and Day 10. Each column represents a sample, and expression intensities reflect the overall transcriptional activity within each tissue and time point. **B** Violin plots illustrating the distribution and density of gene expression (RPKM) in gonadal and whole-worm samples from both wild-type (N2) and reduced insulin/IGF-1 signaling (rIIS) backgrounds. The plots depict the full range of expression levels, including median and interquartile ranges, to highlight overall transcript abundance patterns across conditions. Violin tails represent kernel density estimation. Maximum RPKM values for each group are annotated above the corresponding violins and expressed as multiples of 1000. These annotations represent the true observed maxima, which may extend beyond the visible range of the violin density curves due to kernel smoothing and sparsity at extreme values. **C** Gene classification based on expression specificity. Genes uniquely expressed in gonads were compiled to define a gonad-specific gene set (left panel), whereas the whole-worm gene set was constructed by aggregating transcripts detected across all whole-body transcriptomes (right panel). The middle panel shows the overlap between the gonad and whole-worm gene sets, irrespective of the strain background or sample collection time point. Genes expressed in both gonadal and whole-worm samples were categorized as Shared Gonadal (ShGn), whereas those exclusively detected in whole-worm samples were designated as Non-Gonadal (NoGn). The representation factor (RF) and significance of overlap were calculated via the hypergeometric test

gonads "Non-Gonadal (NoGn), (Fig. 1C). Our goal is to accurately capture gene expression levels in their natural context, minimizing external influences such as gene perturbations or tissue removal. The second category (NoGn) encompasses genes expressed in the entire organism but not in the gonads. While this approach may not encompass every gene expressed throughout an organism, it provides crucial insights into gene expression in its native environment. Notably, a small fraction of genes is "gonad exclusive" (n = 108) were excluded from further analysis because of their low expression levels.

Differential expression dynamics in gonadal and non-gonadal tissues

To examine the differential expression of gonadal genes under rIIS conditions relative to the wild type (WT) across various time points, we selected genes based on the criteria of $p \leq 0.05$ and $\log_2 FC \geq 1$. At the young adult stage (Day 0), only a limited number of shared gonadal genes (ShGn) were differentially expressed, with 60 genes (0.7%) upregulated and 176 genes (2%) downregulated out of 8,414 differentially expressed genes. However, during the peak reproductive period on Day 2, the dynamics shifted dramatically, revealing a significant

increase in differential expression: 554 genes (6.6%) were upregulated, and 868 genes (10.3%) were downregulated from a total of 8,451 expressed genes. In contrast, during the reproductive decline period (Day 6), we observed a significant reduction in differentially expressed genes, alongside a reversal of the previous trend. Here, 406 genes (4.8%) were upregulated, and 306 genes (3.6%) were downregulated out of 8,462 expressed genes. However, at the most advanced stage of reproductive decline (day 10), the number of differentially expressed genes rebounded, closely aligning with the number observed during the active reproductive period on day 2, with 452 genes (5.4%) upregulated and 806 genes (9.6%) downregulated out of 8,430 expressed genes (Fig. 2, left & middle panel).

In the non-gonadal group (NoGn), at the young adult stage (Day 0), 2,139 genes (40%) were upregulated, and 238 genes (4.4%) were downregulated out of 5,359 expressed genes. On Day 10, a total of 1,916 genes (35.7%) were upregulated, and 273 genes (5.1%) were downregulated out of 5,360 expressed genes indicating sustained

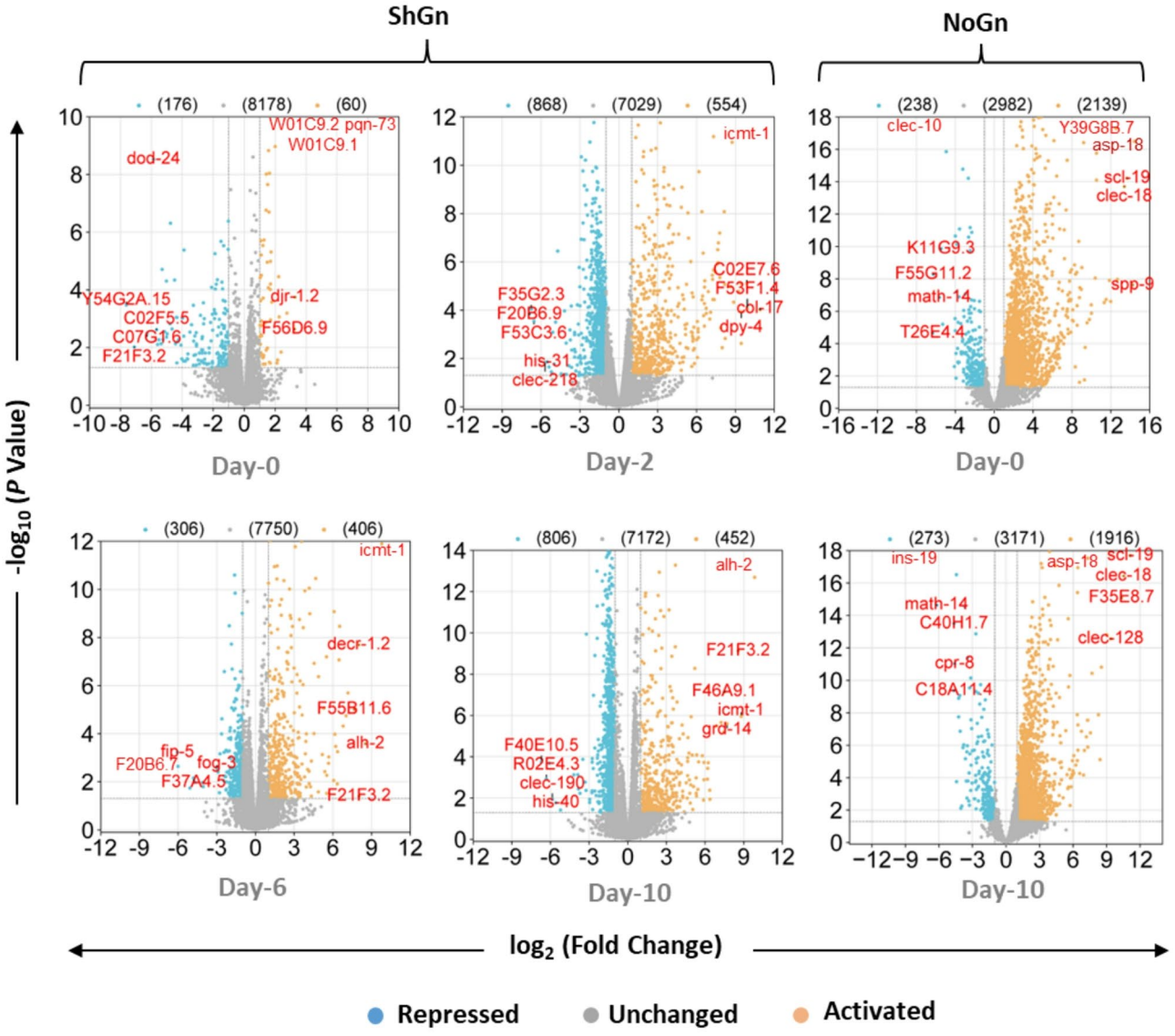

Fig. 2 Differentially expressed genes (DEGs) between the wild-type and rIIS strains across time points. Volcano plots showing DEGs under rIIS conditions compared with the wild type in shared gonads (left and middle panels) and non-gonadal samples (right panels). Each condition represents three biological replicates ($n = 3$), with each replicate consisting of 20 gonads pooled as 4 tubes of 5 gonads each (for gonad samples) or whole-worm samples of the same age. Upregulated genes are indicated as activated (mustard color), downregulated genes as repressed (blue color), and unchanged genes in gray. Gene expression changes are represented by $\log_2$-fold changes on the x-axis, and significance is shown as the $-\log_{10}$ p value on the y-axis. The top five most highly expressed genes in each category are labeled. Differentially expressed genes (DEGs) were identified using the cutoff criteria of $|\log_2 FC| \geq 1$ and $P \leq 0.05$

systemic adaptation despite reproductive decline (Fig. 2, right panel).

We highlighted the top five genes in each category with fold changes ≤ 5 and $p \leq 0.05$ in both the upregulated and downregulated groups. Further, to experimentally validate the transcriptomic trends, we selected ten highly expressed and consistently upregulated or downregulated gonadal genes that were common across all time points for qRT−PCR validation. The expression levels were assessed across Day 1 and Day 10 using three independent biological replicates. All selected genes showed consistent expression patterns with the RNA-seq data, confirming the reliability of transcriptomic trends observed under reduced insulin/IGF-1 signaling (rIIS) conditions (Figure S1B & C).

Self-organizing map (SOM) and hierarchical clustering identifies distinct temporal module reorganization in gonads under rIIS

Self-organizing map (SOM) analysis was used to visualize and compare temporal gene expression patterns between tissues and strains. In these maps, each hexagon represents a group of genes with similar trajectories, and color intensity reflects the direction and magnitude of expression change across time. This approach allows rapid identification of coordinated transcriptional programs and their temporal shifts under rIIS. In the gonadal compartment, the *daf-2* SOM shows a pronounced temporal remapping of expression modules compared with N2. At Day 0, *daf-2* ShGn maps are dominated by contiguous red–orange sectors (strong down-regulation relative to the mean) in the lower half, transitioning to blue sectors (up-regulated) at the top—almost the inverse of the N2 pattern, where early blue dominance is localized to mid- to lower-grid neurons and red patches are more confined. By Day 2, *daf-2* exhibits a dramatic inversion, with extensive blue enrichment in the upper-left module cluster and concentrated red modules at the periphery, suggesting an early, coordinated activation of a large gene set not seen in N2 (Fig. 3A, first two top vs. bottom panels). At Day 6, *daf-2* maintains strong red dominance in central/lower neurons and corresponding blue activation in flanking modules, whereas N2 at this stage shows a more fragmented pattern with alternating red/blue islands. By Day 10, *daf-2* transitions into a broad blue-dominated lower region and upper red sectors, indicating a late-phase reactivation pattern that is both more spatially coherent and more extensive than in N2, which shows a mixed, less defined late-stage pattern (Fig. 3A, last two top vs. bottom panels). Overall, *daf-2* ShGn modules exhibit larger, more cohesive color blocks and clear temporal shifts, indicating well-coordinated transcriptional programs under rIIS.

In non-gonadal tissues, *daf-2* maps (Day 0 and Day 10) reveal smaller shifts in the spatial distribution of expression modules compared with ShGn. At Day 0, the *daf-2* map shows a concentrated red–orange sector in the mid-left region flanked by large light-blue fields, a configuration retained—albeit inverted in polarity—at Day 10, where upper/mid neurons turn dark blue and lower sectors shift toward yellow–orange. This indicates two-state switching in a subset of modules without extensive recruitment of new neuron groups (Fig. 3B, lower panels). In contrast, N2 NoGn maps retain a striped, S-shaped red/blue pattern from Day 0 to Day 10, suggesting a more stable, modular architecture with gradual polarity changes rather than wholesale remapping (Fig. 3B, top panels). Compared with ShGn, both genotypes show less dramatic temporal reorganization in NoGn, consistent with modest transcriptional responsiveness in non-gonadal tissues under rIIS.

Next, we performed correlation-based hierarchical clustering of expression trajectories that uncovered striking differences between shared-gonadal (ShGn) and non-gonadal (NoGn) tissues under reduced insulin/IGF-1 signaling (*daf-2*) compared with wild type (N2). In *daf-2*, six significant distinct ShGn clusters were identified, each characterized by highly coherent temporal profiles. Two major upregulated clusters were identified in *daf-2* gonads (CS3, $n = 330$; CS4, $n = 234$). CS3 was exemplified by the top five *genes hil-1*, *timp-1*, *clx-1*, *dpy-31*, and *clec-83*, spanning chromatin organization, extracellular matrix remodeling, and innate immunity. CS4 showed a sharp induction at Day 2 followed by stabilization, with top representatives *cdr-2*, *fbxc-43*, *fbxa-98*, *osm-3*, and *unc-38*, linked to developmental transcriptional regulation, protein turnover, ciliary transport, and synaptic signaling. Together, these clusters indicate that reduced IIS promotes sustained activation of structural, immune, and neuronal pathways in the gonad (Fig. 3C, lower panels). Two major downregulated clusters (CS1, CS2) showed an immediate decrease from Day 0 to Day 2, followed by partial recovery or sustained repression toward Day 10 (Figure S2B). Smaller clusters (CS5, CS6) exhibited stable high expression or transient Day 2 peaks, indicating specialized temporal programs (Figure S2B). In contrast, N2 ShGn displayed a distinct pattern. The largest cluster (CS1) showed moderate early downregulation followed by stabilization and was represented by *far-8*, *cpr-1*, *ttr-46*, *col-17*, and *cpg-7*, encompassing lipid metabolism, proteolysis, and extracellular matrix components. CS2 was characterized by *pmp-5*, *atf-5*, *elo-5*, *col-81*, and *mlc-3*, spanning lipid metabolism, stress-responsive transcription, collagen, and contractile machinery. The consistent decline of these genes highlights a progressive loss of metabolic and structural capacity in wild-type gonads (Fig. 3C, upper panels), (Fig. 3C, upper panels).

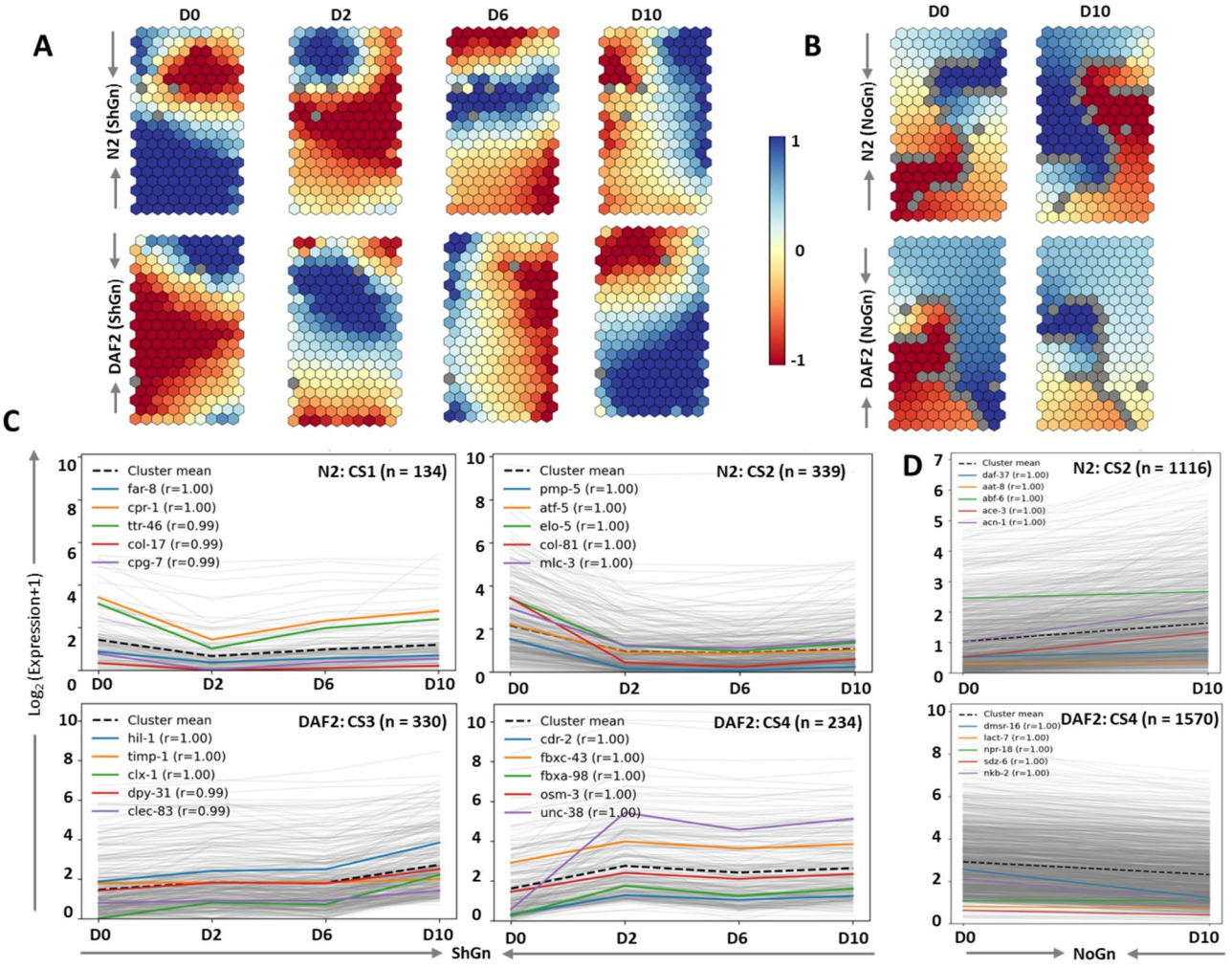

Fig. 3 Self-organizing map (SOM) and hierarchical clustering reveal tissue-specific temporal transcriptional programs under reduced insulin/IGF-1 signaling (rIIS). **A** Self-organizing map (SOM) analysis of normalized expression trajectories (RPKM), (row-wise Z-score, range − 1 to 1) for differentially expressed genes ($|\log_2 FC| \geq 1$, $P \leq 0.05$) across developmental time points. Each hexagon represents a neuron; color indicates mean normalized expression of assigned genes, gray = no assigned genes. Shared-gonadal (ShGn) SOMs for N2 and *daf-2* are shown for Day 0, Day 2, Day 6, and Day 10. **B** Non-gonadal (NoGn) SOMs for N2 and *daf-2* are shown for Day 0 and Day 10. **C** Correlation-based hierarchical clustering (Pearson distance, Ward's linkage) of $\log_2$-transformed RPKM values for the same gene sets. Cluster means (black dashed) are overlaid on individual gene trajectories (light gray, α = 0.15). In ShGn, six distinct temporal clusters are observed each for N2 and *daf-2*. **D** NoGn resolves into four clusters each for N2 and *daf-2*. Cluster numbers were assigned sequentially as generated by hierarchical clustering and do not indicate any biological ranking. Each cluster represents a distinct temporal expression trajectory identified within the ShGn and NoGn groups. The largest clusters have been shown in this figure. Please refer figure S2 for the remaining clusters. Representative genes (top five most correlated with each cluster mean) are highlighted in distinct colors (matplotlib 'Table 10' palette) and labeled

The upregulated clusters (CS4, CS6) exhibited lower amplitude changes and more gradual trends. The smaller clusters (CS3, CS5) showed either sustained or gradual decrease expression (Figure S2A). The strong early induction observed in *daf-2* CS4 was absent in N2, highlighting an rIIS-specific activation program in the gonadal compartment.

Non-gonadal trajectories resolved into four clusters with modest expression changes and relatively flat temporal profiles were observed under rIIS (*daf-2*), compared to ShGn. In *daf-2*, the largest cluster (CS4, $n = 1570$) showed a slight decline, particularly enriched in *dmsr-16*, *lact-7*, *npr-18*, *sdz-6*, and *nkb-2*, comprising neuropeptide receptors, antimicrobial peptides, and stress-response factors. Other clusters CS1 ($n = 879$) and CS2 ($n = 351$) showed sustained increase in expression and the CS4 ($n = 487$) with decline with age (Figure S2D). By contrast, in N2, the largest cluster (CS2, $n = 1116$) was represented by *daf-37*, *aat-8*, *abf-6*, *ace-3*, and *acn-1*, spanning sensory GPCRs, metabolic transporters, antimicrobial peptides, and synaptic regulators. This cluster showed modest induction, reflecting a mixed but less coordinated transcriptional response compared to *daf-2* (Fig. 3D, upper vs. lower panels). Similarly, CS1 ($n = 792$) exhibited a gradual rise; however, both CS1 and CS2 displayed only modest expression levels relative to the high

expression levels seen in *daf-2* (Clusters mean lines). The remaining clusters, CS3 ($n = 501$) and CS4 ($n = 865$), showed gradual age-associated declines (Figure S2C).

Regulatory divergence in gonadal gene expression

To enhance the robustness of our analysis, we applied a more stringent selection threshold of $\log_2$ fold change (FC) ≥ 1.5, generating nonredundant gene lists for each tissue type. This yielded 710 upregulated and 689 downregulated genes in the ShGn group, and 2,255 upregulated and 293 downregulated genes in the NoGn group (Figure S3A, B). We then evaluated the temporal persistence of transcriptional regulation by comparing activated and repressed gene sets across four gonadal and two non-gonadal time points under reduced insulin/IGF-1 signaling (rIIS). In gonadal tissue, the overlap between activated and repressed genes was not statistically significant (RF = 1.3, $p = 0.08$), indicating that genes differentially expressed at earlier stages generally maintained their direction of regulation throughout the lifespan compared to wild-type. In contrast, non-gonadal tissue showed a significant negative enrichment (RF = − 3.58, $p = 4.5 \times 10^{-7}$) for this overlap, indicating an underrepresentation of directional switching (Figure S3A, B). Collectively, these findings suggest that transcriptional programs under rIIS are directionally stable over time, with minimal reversal between activation and repression states.

To determine whether the gonadal environment is more diverse than the rest of the organism, we conducted gene network analyses. Our findings indicate that the reduced insulin/IGF-1 signaling (rIIS) gonadal niche is highly complex and diverse, integrating multiple pathways that regulate the metabolism of various metabolites alongside numerous signaling pathways (Fig. 4).

Our data reveal a significant number of genes associated with metabolic pathways enriched in gonads that corroborate previous findings on longevity enhancement, with major upregulation in pathways related to unsaturated fatty acid biosynthesis [44–46], peroxisomes [47], lysosomes [48] and autophagy [49]. As anticipated, genes associated with FoxO signaling and longevity regulation are upregulated in the gonads. Interestingly, major signaling pathways, including the TGF-β, mTOR, MAPK, Hippo, Notch, Wnt, and ErbB signaling pathways, are predominantly downregulated. Furthermore, pathways related to endocytosis, axon regeneration, and oxidative phosphorylation were also downregulated. This finding indicates a complex interplay between insulin signaling and various pathways that govern growth, metabolism, and cellular health in the gonads, potentially influencing reproductive outcomes and overall organismal vitality. At the organismal level, we observed that most metabolic pathways were upregulated, like those in the gonads, whereas some signaling pathways, such as ErbB and Wnt, were also upregulated, in contrast with the gonadal findings. Moreover, gonad complexity was not evident at the whole-worm level (Fig. 5A). Quantitative assessment of network complexity revealed that the shared gonad (ShGn) network comprised 216 nodes, 360 edges, and 48 enriched pathways, whereas the non-gonadal (NoGn) network contained 128 nodes, 255 edges, and 31 pathways, indicating a higher degree of connectivity and functional diversity in the ShGn network (Figure S4A).

Next, we investigated whether the regulation of these genes differed between the ShGn and NoGn groups. Transcription factor enrichment analysis was then conducted via the AnnoMiner tool, which evaluates promoter regions for each transcription factor (TF) on the basis of binding density, considering 1,000 bp upstream and 50 bp downstream from the transcription start site (TSS). Gonadal genes presented significantly higher enrichment scores for specific transcription factors (TFs) than did the entire worm-exclusive gene set (NoGn), indicating tighter regulatory control. Many of the upregulated and downregulated genes in the gonads were regulated by distinct TFs, whereas the same TFs primarily governed the most differentially expressed genes within the NoGn group. These findings suggest a complex regulatory network tailored to reproductive needs in the gonads. Furthermore, the presence of additional TFs regulating gonadal genes that are not enriched in the NoGn group points to specialized mechanisms crucial for reproductive success (Fig. 5B).

GO enrichment highlights distinct gonadal and non-gonadal gene programs under rIIS

GO enrichment analysis revealed distinct and tissue-specific biological processes associated with activated and repressed genes under reduced insulin/IGF-1 signaling (rIIS). In gonadal tissue (ShGn), activated genes (Fig. 6A) were enriched for immune-related and developmental processes, including innate immune response, defense response to Gram-positive bacterium, cell death, and anatomical structure development. These were complemented by strong enrichment for structural and extracellular components such as collagen trimer and structural constituent of cuticle, as well as catalytic activities like aspartic-type and cysteine-type endopeptidase activity. In contrast, repressed genes (Fig. 6B) were predominantly associated with transcriptional regulation (regulation of transcription, DNA-templated; sequence-specific DNA binding), developmental processes (nematode larval development; cell differentiation), and nuclear/chromatin-related components (nucleosome, nucleus), indicating downregulation of transcriptional and developmental

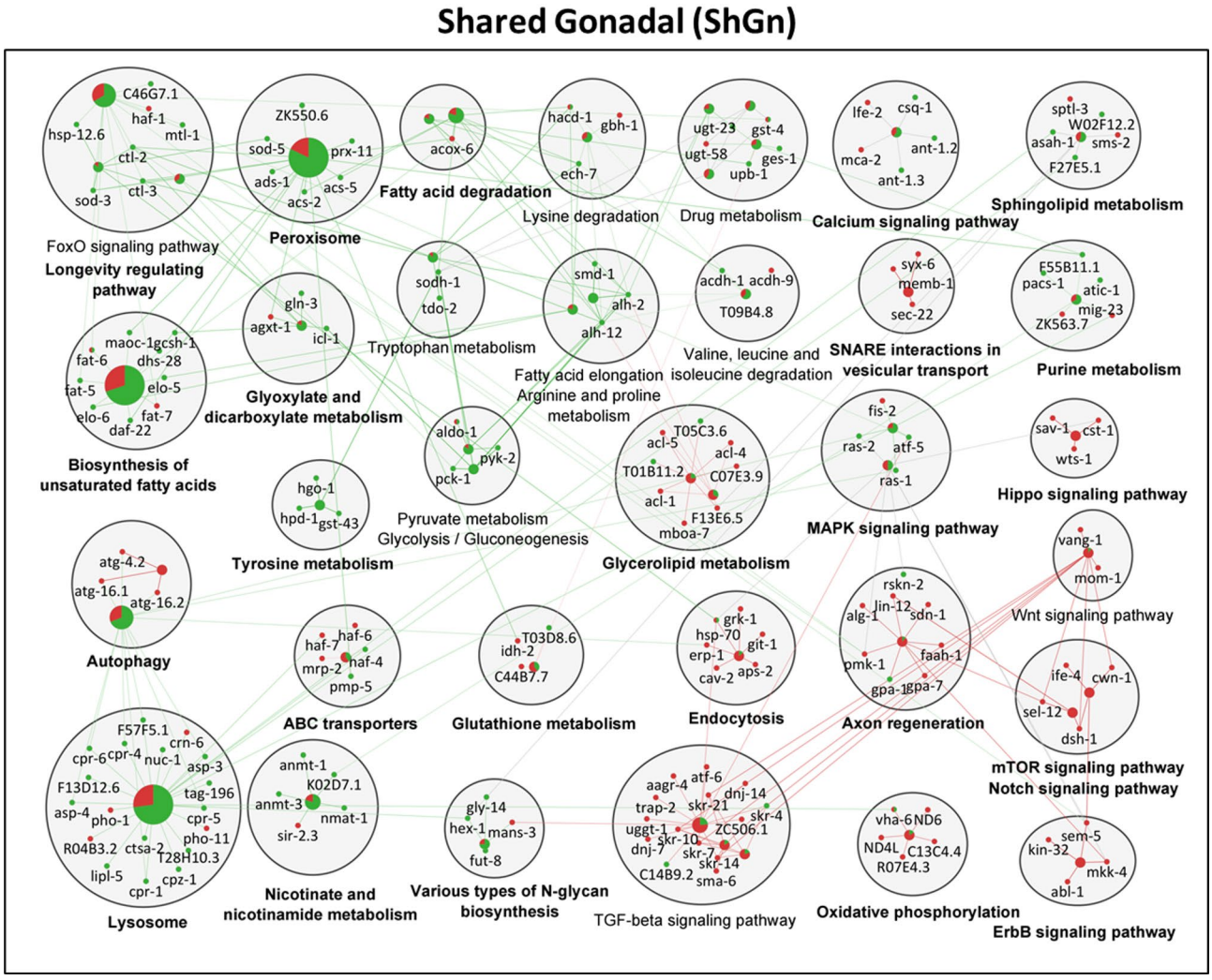

Fig. 4 Regulatory divergence in gonadal (ShGn) gene expression. Gene groups with predominantly activated (upregulated) genes are aligned to the left side (green color), whereas groups with mainly repressed (downregulate) genes are positioned on the right side (red color) for clearer visualization. The size of the smaller circles at the center of each large cluster corresponds to the number of genes involved in each signaling pathway. The outer circles surrounding these groups have been manually adjusted for visual clarity, and edge lengths do not represent correlations or interaction strengths between genes; rather, they have been modified solely to enhance layout readability. The signaling pathways shown in bold indicate greater statistical significance. Gene network analysis of DEGs was performed via Cytoscape with the ClueGO v2.5.8 plugin for network analysis. Differentially expressed genes (DEGs) were identified using the cutoff criteria of $|\log_2 FC| \geq 1.5$ and $P \leq 0.05$

programs. In non-gonadal tissue (NoGn), activated genes (Fig. 6C) were enriched for xenobiotic and metabolic processes (xenobiotic metabolic process, organic acid metabolic process, steroid hydroxylase activity), immune functions (innate immune response), and extracellular or membrane-associated terms (pseudopodium, extracellular region, integral component of membrane). Key molecular functions included heme binding, monooxygenase activity, and oxidoreductase activity. Repressed genes (Fig. 6D) showed enrichment for developmental (embryo development, cell fate specification), immune (innate immune response, defense response to Gram-positive bacterium), and lipid transport regulation processes (negative regulation of fatty acid transport), as well as membrane-associated and catalytic functions such as membrane raft, UDP-glycosyltransferase activity, and glucuronosyltransferase activity. Collectively, these findings indicate that rIIS elicits strong, tissue-specific transcriptional programs: gonadal activation centers on structural and reproductive functions, whereas non-gonadal activation is biased toward metabolic adaptation and xenobiotic clearance. Repression patterns reflect selective suppression of transcriptional, developmental, and certain metabolic pathways, underscoring a coordinated, tissue-tailored reprogramming of gene expression under rIIS.

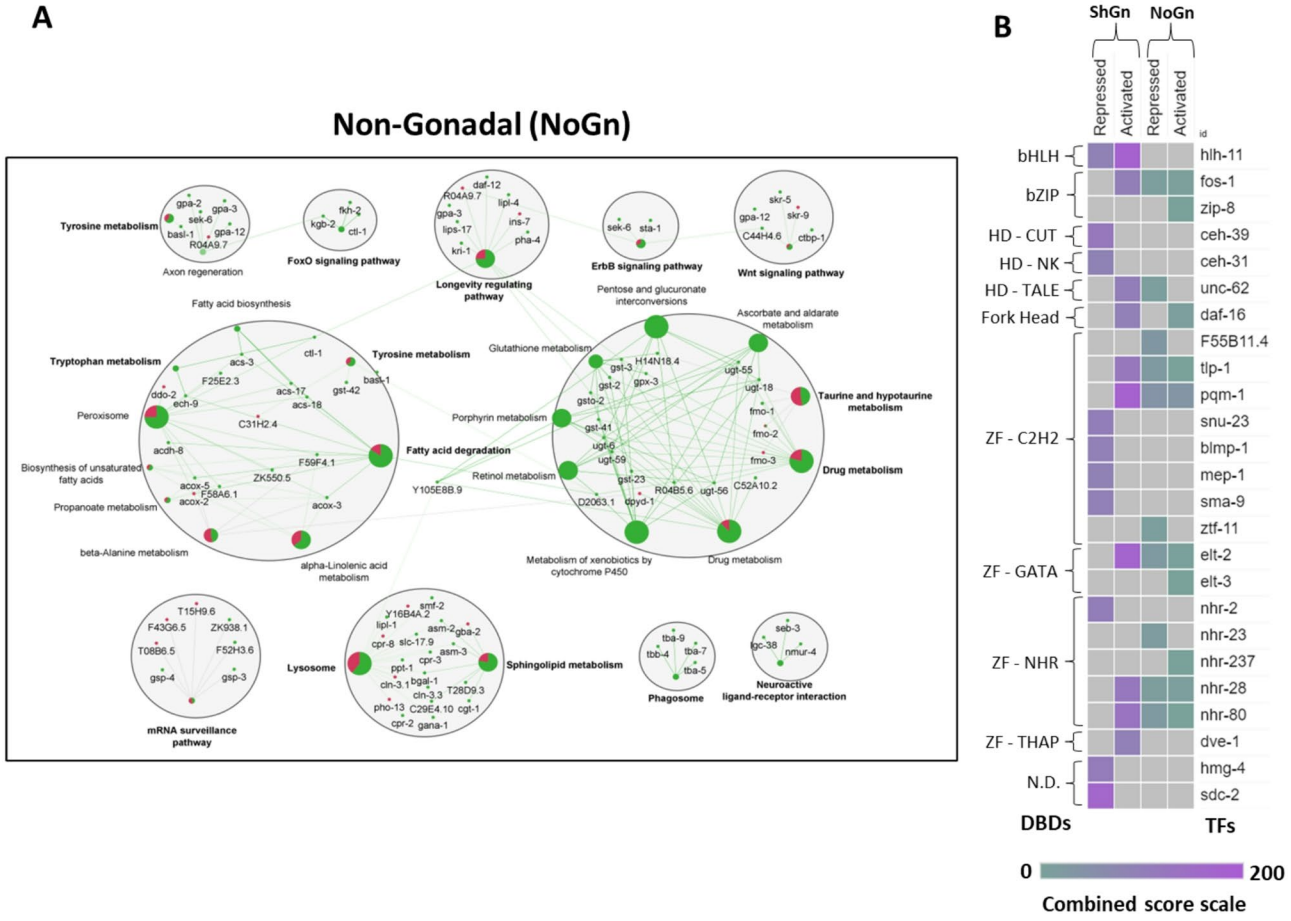

Fig. 5 Systems-level analyses of non-gonadal gene networks and transcription factor enrichment. **A** Network analysis of the non-gonadal (NoGn) dataset revealed that most upregulated genes are associated with metabolic pathways, with additional contributions from signaling pathways such as ErbB and Wnt. Compared with the gonadal network, the systemic (organismal) network exhibited reduced regulatory complexity, consistent with more generalized transcriptional control in non-reproductive tissues under reduced insulin/IGF-1 signaling (rIIS). **B** Transcription factor (TF) enrichment analysis performed across the entire dataset (ShGn and NoGn). TFs were classified according to DNA-binding domain (DBD) families, and their relative enrichment was estimated using the enrichment score formula: (list hits/list size)/(genome hits/genome size), implemented in the AnnoMiner tool. The combined enrichment score (enrichment score × –log(P-value)) is shown as a heatmap, highlighting differential TF enrichment between ShGn and NoGn conditions. Differentially expressed genes (DEGs) were identified using the cutoff criteria of $|\log_2 FC| \geq 1.5$ and $P \leq 0.05$

Cross-study validation and human ortholog mapping of differentially expressed genes under rIIS

To benchmark our dataset, we compared the IIS-dependent ShGn- and NoGn-enriched transcripts with previously published germline and gonadal profiles (Ortiz et al. 2014; Lee et al. 2017; Mei Han et al. 2019). For the ShGn-enriched set, we identified 710 upregulated and 689 downregulated genes. Among the upregulated genes, 381/710 (53.7%) overlapped only with Ortiz et al. (2014), 164/710 (23.1%) were unique to this study, and 165/710 (23.2%) overlapped with either Mei Han 2019 or Lee 2017 (Fig. 7A). For the downregulated set, 135/689 (19.6%) overlapped only with Ortiz, 101/689 (14.7%) were unique, and the majority (453/689; 65.7%) overlapped with Mei Han and/or Lee (Fig. 7B). These results indicate that ShGn expression substantially refines earlier gonadal datasets while also contributing a distinct IIS- and age-dependent gene set (~15–23%) unique to our study. By contrast, in the NoGn fraction, we identified 2,255 upregulated and 293 downregulated genes. The majority (1,690/2,255; 74.9% upregulated and 182/293; 62.1% downregulated) did not overlap with any previously reported gonadal/germline datasets (Figure S4B and C). This pattern is consistent with the design of the NoGn dataset, which was derived after excluding gonad-specific transcripts, and therefore expectedly shows little overlap with germline-focused resources. This observation validates the accuracy of our tissue-partitioning strategy and underscores that the NoGn set reflects somatic transcriptional programs largely absent from gonadal datasets. Together, these analyses demonstrate that ShGn captures both conserved and IIS-dependent gonadal signals, while the NoGn dataset provides a clean separation of somatic

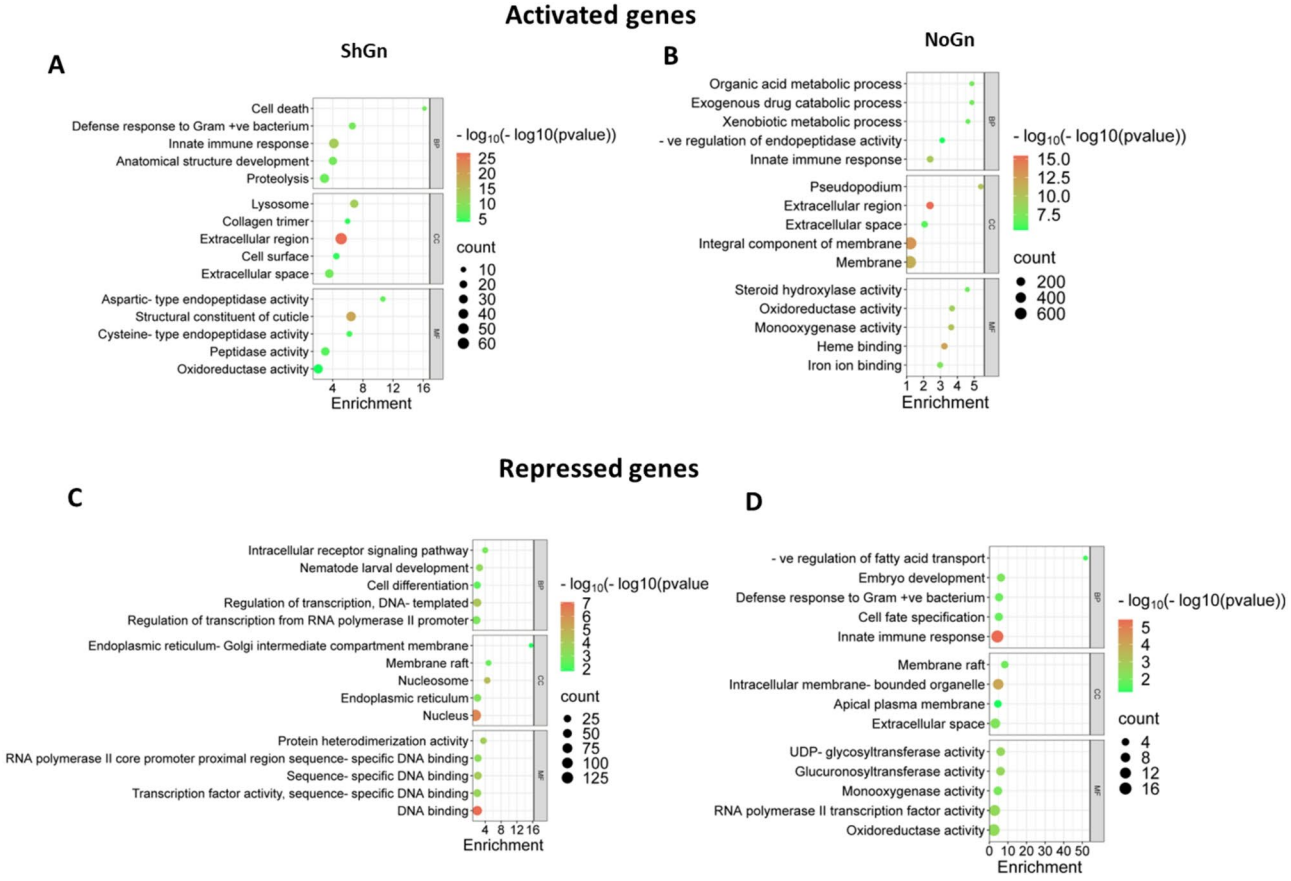

Fig. 6 GO enrichment analysis of activated (upregulated) and repressed (downregulated) genes in gonadal (ShGn) and non-gonadal (NoGn) tissues under reduced insulin/IGF-1 signaling (rIIS). Panels **A** and **B** show the top enriched Gene Ontology (GO) terms for activated genes in ShGn and NoGn, respectively. Panels **C** and **D** show the top enriched GO terms for repressed genes in ShGn and NoGn, respectively. Enrichment scores are plotted as $-\log_{10}$(p-value), and terms are color-coded according to GO category: biological processes (BP), cellular components (CC), and molecular functions (MF). Differentially expressed genes (DEGs) were identified using the cutoff criteria of $|\log_2 FC| \geq 1.5$ and $P \leq 0.05$

expression, thereby offering complementary insights into tissue-specific aging trajectories.

We next examined the evolutionary conservation of these IIS-regulated gene sets across nine orthology databases. A clear distinction was observed between gonadal (ShGn) and non-gonadal (NoGn) IIS-regulated genes in terms of evolutionary conservation. Across all nine orthology databases, ShGn transcripts displayed consistently higher levels of conservation compared to NoGn transcripts. Within the gonadal fraction, 20–25% of activated genes and 31–35% of repressed genes could be assigned human orthologs, indicating that nearly one-third of IIS-repressed gonadal genes represent deeply conserved modules. In contrast, conservation within the non-gonadal fraction was substantially lower, with only 10–17% of activated genes and 8–20% of repressed genes showing orthology (Fig. 7C). This pattern was robust across databases, with ShGn consistently exceeding NoGn by 8–15% points for activated genes and by 12–15% points for repressed genes. These differences highlight a strong tissue-specific hierarchy of conservation within IIS transcriptional programs. The gonadal fraction is enriched for evolutionarily constrained transcripts that likely underpin fundamental reproductive processes. By contrast, the non-gonadal fraction, although transcriptionally responsive to IIS, is composed of genes with markedly lower conservation, consistent with a more variable, lineage-flexible program.

Discussion

Genetic mutations in several signaling pathways that regulate longevity have been implicated in delaying reproductive aging; however, these mutations are often accompanied by a significant reduction in total progeny production [8, 13, 14, 50]. Previous studies, together with our data, have demonstrated that insulin/IGF-1 signaling (IIS) mutants exhibit a distinct phenotype characterized by an extended reproductive period with a nearly wild-type brood size under permissive temperature conditions [13, 51, 52]. Moreover, early progeny production has been shown to neither accelerate nor delay the duration of the reproductive period, suggesting that early fecundity is

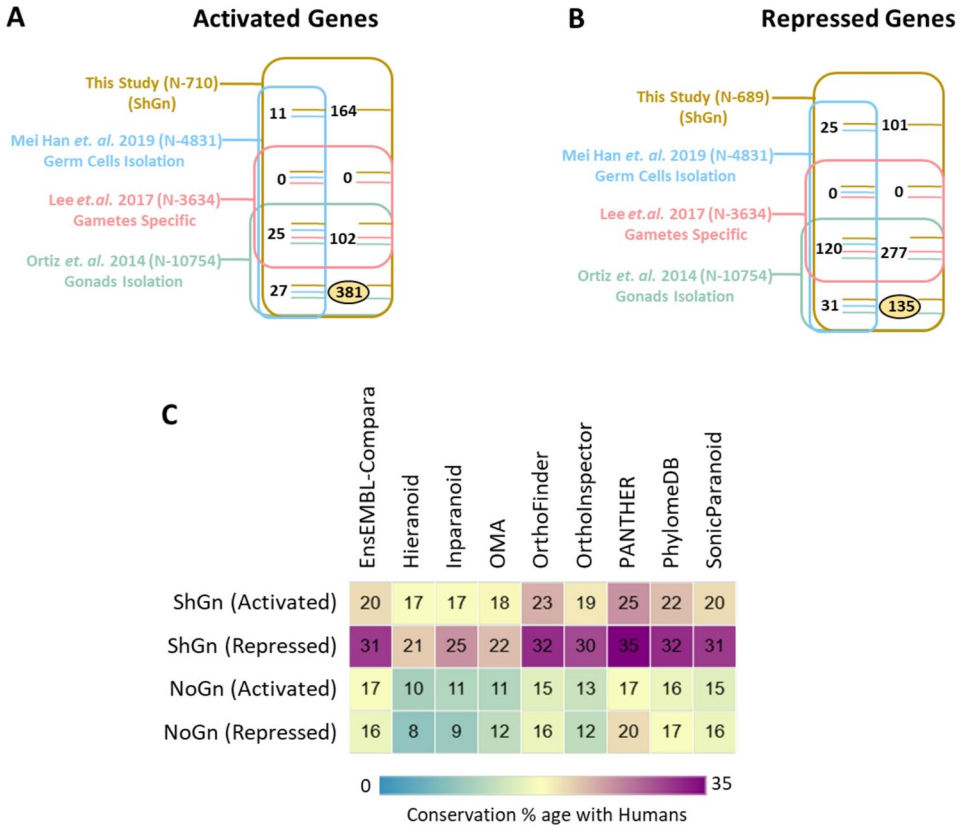

Fig. 7 Comparative analysis of gonadal transcriptional profiles and conservation with humans. **A** Venn diagram showing the overlap of activated (upregulated) genes identified in this study (ShGn; $N = 710$) with published datasets focused on germ cell, gamete-specific, and whole-gonad gene sets. A total of 381 genes overlapped with earlier gonadal datasets. **B** Venn diagram showing the overlap of repressed (downregulated) genes identified in this study (ShGn; $N = 689$) with the same reference datasets. A total of 135 genes overlapped with earlier gonadal datasets. **C** Heatmap summarizing the conservation of ShGn and NoGn differentially expressed genes with humans across nine orthology databases: Ensembl-Compara, Hieranoid, InParanoid, OMA, OrthoFinder, OrthoInspector, PANTHER, PhylomeDB, and SonicParanoid. Values represent the percentage of conserved genes. Differentially expressed genes (DEGs) were identified using the cutoff criteria of $|\log_2 FC| \geq 1.5$ and $P \leq 0.05$

not a direct determinant of reproductive longevity [13]. Based on these findings, we focused our investigation on the IIS pathway as a key modulator of reproductive aging.

To understand how gonads differ in function compared with the rest of the organism, it is essential to investigate conditions where gonads are absent but the rest of the organism remains intact. However, the inhibition of early gonadal development induces alterations in other organs, which are attributable to the interorgan communication network (ICN), in which organs release factors that influence the physiology of cells in distant tissues [33]. Consequently, mutant worms lacking gonads during development may exhibit pleiotropic effects or compensatory mechanisms that complicate the identification of true gene expression in their native state. Additionally, these mutants have genetic backgrounds or physiological changes unrelated to gonadal development, potentially introducing artifacts into the analysis. Therefore, to capture the native expression of genes, we examined both dissected gonads and whole worms (which included intact gonads). Furthermore, to prevent contamination from sperm and developing embryos, gonads were dissected above the spermatheca.

To guide interpretation, we provide an overview of our study design and analytical framework (Fig. 8). Our approach combined precise gonadal dissections with whole-worm profiling, followed by RNA-seq and a tiered analysis strategy. Primary analyses ensured data quality through read trimming, filtering, alignment, and mapping. Secondary analyses normalized expression, assessed sample correlations, and identified differentially expressed genes. Tertiary systems-level analyses—including SOM profiling, clustering, network construction, functional enrichment, and conservation mapping—revealed stage-specific remodeling and evolutionary constraints. This framework provides a structured lens through which to interpret how rIIS reshapes gonadal transcriptional programs and links reproductive aging to systemic longevity.

Using this approach, our study uncovered several key insights. Our analysis reveals that the gonadal transcriptional program under rIIS is both temporally dynamic

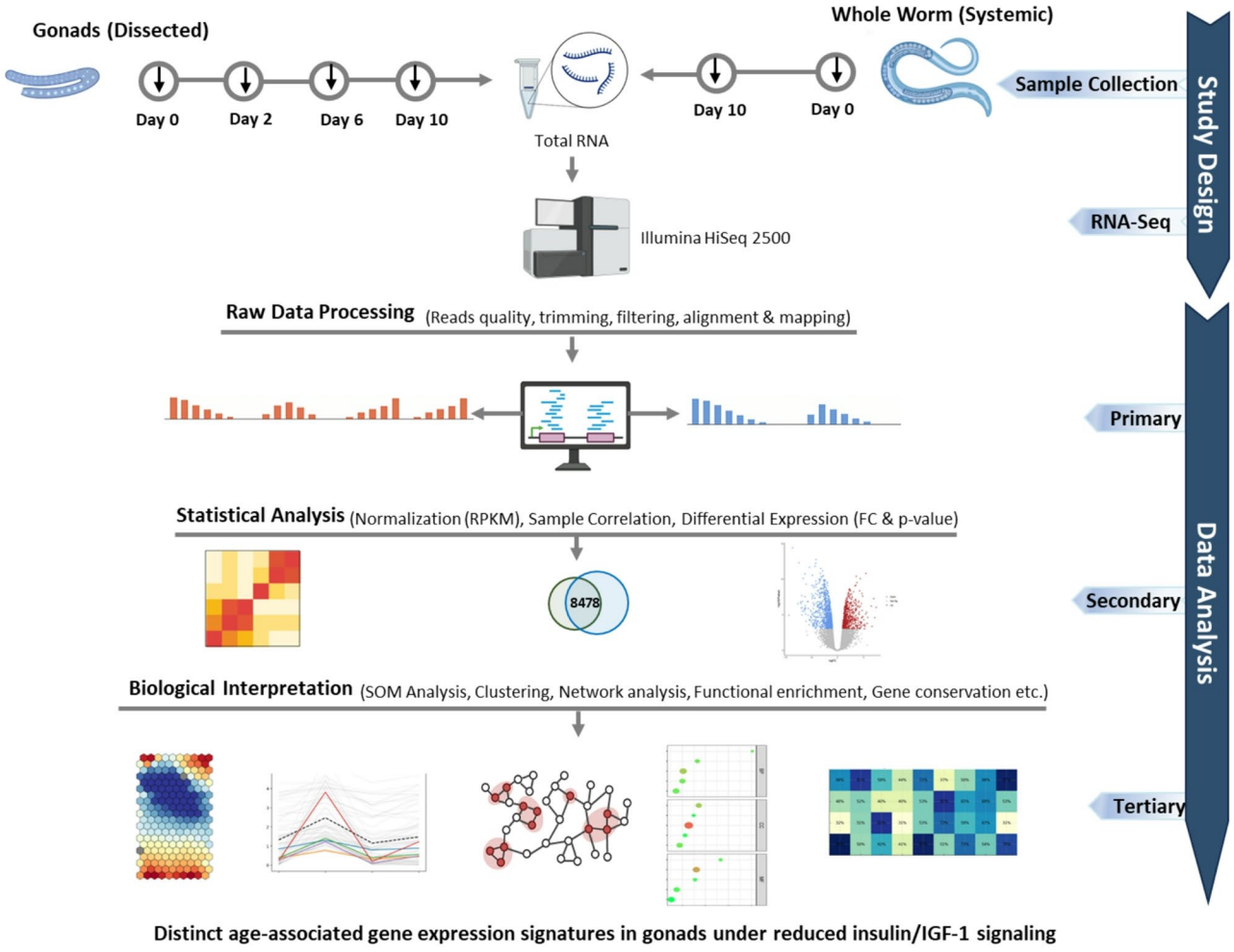

Fig. 8 Tiered analytical workflow for resolving gonadal versus systemic transcriptional programs under reduced insulin/IGF-1 signaling (rIIS). The schematic outlines the sequential framework used in this study. The upper panel depicts the experimental design, including sample collection strategy and RNA sequencing. Data analysis was structured into three tiers: (i) Primary analysis, involving quality control of raw reads (trimming, filtering, alignment, and genome mapping) to generate high-confidence datasets; (ii) Secondary analysis, including expression normalization (RPKM), sample correlation assessment, and identification of differentially expressed genes (DEGs) using statistical thresholds; and (iii) Tertiary analysis, integrating systems-level approaches such as self-organizing maps (SOM) for temporal dynamics, hierarchical clustering for gene modules, network analysis of pathway interactions, functional enrichment to annotate biological processes, and cross-species conservation analysis to assess evolutionary relevance

and highly regulated, contrasting with the broader systemic responses observed at the whole-organism level. The gonad exhibited minimal differential expression at the young adult stage, reflecting a period of transcriptional stability as reproductive maturity is established. However, by Day 2—the peak of fertility—there was a dramatic remodeling of the transcriptome, marked by extensive activation and repression of shared gonadal (ShGn) genes. This surge likely reflects heightened transcriptional demands for gamete production and reproductive signaling, consistent with prior reports that reproductive peak coincides with activation of biosynthetic and metabolic pathways critical for fertility. Interestingly, by Day 6, when reproductive decline begins, the overall number of differentially expressed genes was reduced, accompanied by a reversal in the earlier activation trend. This suggests a shift in gonadal priorities away from reproduction toward resource reallocation, potentially buffering somatic maintenance as fertility wanes. By Day 10, however, transcriptional activity rebounded, with large numbers of genes once again differentially expressed (Fig. 2). Such late-life reactivation may represent compensatory transcriptional programs attempting to sustain residual reproductive capacity despite declining fecundity. In contrast, non-gonadal (NoGn) datasets revealed a markedly different pattern: systemic transcription was dominated by widespread gene upregulation both at Day 0 and Day 10, reflecting strong growth and metabolic activity early in life and persistent organismal maintenance later. This disparity underscores a key divergence between gonadal and somatic transcriptional strategies: while systemic tissues maintain activation programs that

support overall organismal survival, the gonad engages in sharp, stage-dependent switches, with periods of strong activation followed by repression and compensatory rebound. Notably, the predominance of repressed genes in gonads compared with systemic upregulation suggests that reproductive tissues may be more sensitive to age-associated transcriptional decline, even under protective rIIS conditions. The early and coordinated remodeling of *daf-2* gonads by Day 2 (Fig. 2) suggests that the IIS pathway establishes transcriptional control well before overt phenotypic differences in reproductive output arise. This observation aligns with prior reports that *daf*-2 mutants show precocious activation of stress-response and maintenance pathways [14, 23, 51, 53, 54]. However, our data extend these findings by showing that such responses are highly tissue-specific and the gonad displayed sharp, coordinated transitions. This distinction underscores the importance of tissue-resolved analyses, as averaging across whole animals can obscure critical regulatory events.

The SOM analysis reveals that rIIS elicits an early and highly coordinated transcriptional reprogramming in the gonad, in contrast to the gradual and fragmented adjustments in wild type (Fig. 3A). Such sharp transitions at earlier stages suggest that IIS acts as a timing mechanism, rapidly establishing transcriptional states that persist across reproductive life. This spatial coherence of expression modules in *daf-2* gonads indicates that IIS does not simply modulate individual genes but orchestrates broad gene networks, consistent with models of IIS downstream TFs acts as a master regulators of chromatin and transcriptional architecture [55]. In contrast, non-gonadal tissues exhibited only modest module switching under rIIS, underscoring that the reproductive system functions as a signaling hub for aging, consistent with studies showing that somatic gonadal tissues regulate systemic lifespan through steroid signaling and that germline signals modulate peripheral DAF-16 activity [56, 57]. These findings indicate that rIIS induces early, coordinated transcriptional remodeling in the gonad, underscoring its sensitivity to IIS and contribution to reproductive longevity. It also appears to represent a complementary, tissue-specific adaptation linking reproductive function with aging. Moreover, the temporal trajectories under rIIS are distinct, coherent, and directionally stable, indicating that rIIS establishes persistent regulatory states in the gonad. Chromatin-mediated control appears central to this process too, as reductions in H3K9me1/2 methylation enhance DAF-16 activity and extend lifespan in *daf-2* mutants [58], while other chromatin modifiers H3K27regulate longevity through changes in accessibility and transcriptional output [59]. The SWI/SNF complex has similarly been shown to be modulated by DAF-16 transcription factor, linking chromatin remodeling to sustained IIS-dependent effects [55]. Consistent with these findings, we identified several chromatin modulating genes (e.g., *hil-1*, *hil-3*, *his-37*, *mef-2*) within strongly regulated clusters (Fig. 3C, S2B), suggesting that rIIS promotes reproductive longevity in part through chromatin-level regulation in the gonad.

Pathway-level analyses displayed strong upregulation of maintenance-related pathways—including unsaturated fatty acid biosynthesis, peroxisomes, lysosomes, and autophagy [48, 60–62]—accompanied by coordinated repression of major growth and developmental cascades such as TGF-β, MAPK, mTOR, and Notch signaling in rIIS gonads. This is consistent with previous work showing that DAF-16 modulates TGF-β/BMP and mTORC1 pathways to control germline proliferation [63], and that components of MAPK and mTOR pathways exhibit dynamic age-dependent regulation [64]. Additionally, DBL-1/BMP signaling is known to influence reproductive aging, with inactivation extending reproductive span independently of IIS [65]. This transcriptional reprogramming suggests that the gonad actively shifts resources from growth and developmental plasticity toward metabolic maintenance and repair, consistent with models linking reproductive tissues to the systemic regulation of aging. By contrast, at the whole-organism level, metabolic upregulation was evident but signaling repression was less pronounced, with certain cascades (e.g., Wnt, ErbB) remaining activated (Figs. 5 and 5A and A). Thus, the gonadal transcriptional landscape appears more specialized, integrating metabolic resilience with a deliberate dampening of proliferative signals—features that may underlie its unique sensitivity to IIS. Transcription factor (TF) enrichment analyses provided further evidence for gonad-specific regulatory complexity. Gonadal genes were governed by a broader and more diverse set of TFs compared with non-gonadal genes, suggesting tighter and more modular control of expression programs. Interestingly, while the most differentially expressed NoGn genes were regulated by a relatively narrow set of TFs, the gonadal repertoire included additional regulators, pointing to specialized transcriptional mechanisms tuned to reproductive function (Fig. 5B). This aligns with the idea that reproductive tissues require finely tuned gene networks to balance gamete production, resource allocation, and stress resilience.

Comparison with previous gonadal datasets highlights both shared and novel features. More than half of our ShGn-enriched transcripts overlapped with Ortiz et al. (2014), validating the robustness of our approach. However, ~23% of upregulated and ~15% of downregulated genes were unique to this study, reflecting the added dimensions of IIS perturbation and temporal sampling. These unique transcripts may represent IIS- and age-dependent programs that were not captured in

prior datasets. By contrast, the non-gonadal (NoGn) set showed minimal overlap with gonad-derived resources, as expected, confirming the success of our tissue-partitioning design. Finally, comparative ortholog analyses demonstrated that IIS-regulated gonadal genes are more evolutionarily conserved than their non-gonadal counterparts, highlighting a conserved regulatory core of reproductive aging. This suggests that reproductive aging under IIS control mobilizes gene networks that are evolutionarily constrained, possibly reflecting the central importance of gonadal integrity for species survival. Together, these results advance our understanding of how IIS shapes reproductive longevity. By resolving gonadal versus organismal responses across adulthood, we show that the gonad is both the primary site and a conserved nexus of IIS-dependent transcriptional regulation. These insights integrate reproductive aging into the broader framework of IIS biology, providing candidate gene sets and conserved modules for future functional investigation.

Conclusion

Our study provides a comprehensive, tissue-resolved view of how reduced insulin/IGF-1 signaling (rIIS) shapes reproductive aging in *C. elegans*. By combining temporally sampled dissected gonads with whole-worm profiles, we demonstrate that the gonad mounts an early, coordinated, and directionally stable transcriptional response to rIIS, in sharp contrast to the broader but less coherent systemic programs. Gonadal remodeling was most pronounced at the reproductive peak, with rIIS activating metabolic maintenance pathways and repressing growth-related signaling cascades, accompanied by enrichment of chromatin regulators that likely enforce long-term transcriptional states. These findings highlight the gonad's unique regulatory complexity, with broader transcription factor control and evolutionary conservation compared to non-gonadal tissues, underscoring its specialized role in linking reproduction to aging. Comparison with prior datasets validated established modules while uncovering distinct IIS- and age-dependent gene sets, offering new candidates for functional dissection. Together, our results position the gonad as a conserved and highly sensitive tissue target of IIS, where transcriptional reprogramming integrates reproductive function with organismal longevity.

Abbreviations

AMA	Advanced Maternal Age
CGC	Caenorhabditis Genetics Center
DAF-16	Dauer Formation Protein-16
DIC	Differential Interference Contrast
ECM	Extracellular Matrix
FDR	False Discovery Rate
GO	Gene Ontology
ShGn	Shared Gonadal Genes (ShGn)
HPG	Hypothalamic-Pituitary-Gonadal
HSF-1	Heat Shock Factor 1
IIS	Insulin/Insulin-Like Growth Factor Signaling
LB	Luria–Bertani
NGM	Nematode Growth Medium
NoGn	Non-gonadal Genes
OP50	E. coli OP50 Strain
PCA	Principal Component Analysis
qRT–PCR	Quantitative Real-time Polymerase Chain Reaction
RIN	RNA Integrity Number
rIIS	Reduced Insulin/IGF-1 Signaling
RNAi	RNA Interference
RPKM	Reads Per Kilobase of Exon Model Per Million Map Read
SKN-1	Skinhead Family Transcription Factor
TF	Transcription Factor
YA	Young Adult

Supplementary Information

The online version contains supplementary material available at https://doi.org/10.1186/s12964-025-02510-7.

Supplementary Material 1.

Supplementary Material 2.

Supplementary Material 3.

Supplementary Material 4.

Acknowledgements

We thank Dr. Arnab Mukhopadhyay, Molecular Aging Laboratory, National Institute of Immunology (NII), New Delhi, India, for his generous support with the experiments and for providing the daf-2 (e1370), rde-1(-), and inx-8::rde-1 strains. His valuable suggestions significantly contributed to the conceptual and experimental advancement of this study. We are also grateful to all the members of the Molecular Aging Laboratory for their technical assistance and continuous support. We acknowledge Dr. Awadhesh Pandit and the sequencing team at the National Centre for Biotechnology Information (NCBI) for their assistance with bulk RNA sequencing. Some strains used in this study were provided by the Caenorhabditis Genetics Center (CGC).

Authors' contributions

Conceptualization and design: NK, AH, SG, SVData curation: NK, SK, SRData acquisition: SR, NK, NKsFunding acquisition: NKInvestigation: NKs, SR, NKMethodology: NK, MS, DP, SV, SuGSupervision and resources: AH, SG, DP, MS, SVSoftware: NKs, NK, VJ, SG, SuG, MSBioinformatics analysis: NKs, NK, VJ, SK, SGExperimental work: NKs, SR, Writing – original draft: NK, NKs, SRWriting – review and editing: All authorsAll the authors have read and approved the final manuscript.

Funding

This study was supported by extramural funding from the Indian Council of Medical Research (ICMR), New Delhi, India (Ref No. 5/10/FR/57/2020-RBMCH), and an intramural grant from the All-India Institute of Medical Sciences (AIIMS), New Delhi (Ref No. A-1032).

Data availability

The datasets generated and analyzed during the current study are available from the corresponding author upon reasonable request. Bulk RNA sequencing data for both gonadal and whole worm samples have been deposited in the National Center for Biotechnology Information (NCBI) Sequence Read Archive (SRA) under BioProject accession number PRJNA1182507 (SUB14831808).

Declarations

Ethics approval and consent to participate

The study was approved by the Institute Ethics Committee of All India Institute of Medical Sciences (AIIMS), New Delhi (Ref No. IEC-120/06.02.2020, dated 09/03/2020). Ethical approval was obtained as part of the institutional

protocol, although specific consent to participate was not needed, as the research involved a model organism, which is exempt from human ethical review requirements.

Consent for publication
Not applicable.

Competing interests
The authors declare no competing interests.

Author details
[1]Department of Reproductive Biology, All India Institute of Medical Sciences, Ansari Nagar, New Delhi 110029, India
[2]Duke Molecular Physiology Institute, 300 North Duke Street, Durham, NC 27701, USA
[3]Division of Neuroscience and Ageing Biology, CSIR-Central Drug Research Institute, Lucknow 226031, India
[4]Emory Healthcare, Emory University, Atlanta, Georgia, 30322, USA

Received: 23 June 2025 / Accepted: 26 October 2025
Published online: 15 December 2025

References

1. Schmidt L, Sobotka T, Bentzen JG, Nyboe Andersen A. ESHRE reproduction and society task force demographic and medical consequences of the postponement of parenthood. Hum Reprod Update. 2012;18:29–43.
2. Bhasin S, Kerr C, Oktay K, Racowsky C. The implications of reproductive aging for the health, vitality, and economic welfare of human societies. J Clin Endocrinol Metab. 2019;104:3821–5.
3. Duncan FE, Confino R, Pavone ME. Female reproductive aging: from consequences to Mechanisms, Markers, and treatments. Conn's handbook of models for human aging. Elsevier; 2018. pp. 109–30.
4. Te Velde ER, Pearson PL. The variability of female reproductive ageing. Hum Reprod Update. 2002;8:141–54.
5. Goud P, Goud A, Van Oostveldt P, Van der Elst J, Dhont M. Fertilization abnormalities and pronucleus size asynchrony after intracytoplasmic sperm injection are related to oocyte postmaturity. Fertil Steril. 1999;72(2):245–52.
6. Hodges CA, Revenkova E, Jessberger R, Hassold TJ, Hunt PA. SMC1β-deficient female mice provide evidence that cohesins are a missing link in age-related nondisjunction. Nat Genet. 2005;37:1351.
7. Lamb N, Sherman S, Hassold T. Effect of meiotic recombination on the production of aneuploid gametes in humans. Cytogenet Genome Res. 2005;111:250–5.
8. Luo S, Kleemann GA, Ashraf JM, Shaw WM, Murphy CT. TGF-β and insulin signaling regulate reproductive aging via oocyte and germline quality maintenance. Cell. 2010;143:299–312.
9. Morita Y, Tilly JL. Oocyte apoptosis: like sand through an hourglass. Dev Biol. 1999;213:1–17.
10. Anderson RA, Marston AL, Telfer EE. Oocyte development: it's all about quality. Reprod Biomed Online. 2025;50:104804.
11. Immediata V, Ronchetti C, Spadaro D, Cirillo F, Levi-Setti PE. Oxidative stress and human ovarian response—from somatic ovarian cells to oocytes damage: a clinical comprehensive narrative review. Antioxidants. 2022;11:1335.
12. Scharf A, Pohl F, Egan BM, Kocsisova Z, Kornfeld K. Reproductive aging in *Caenorhabditis elegans*: from molecules to ecology. Front Cell Dev Biol. 2021;9:718522.
13. Hughes SE, Evason K, Xiong C, Kornfeld K. Genetic and pharmacological factors that influence reproductive aging in nematodes. PLoS Genet. 2007;3:e25.
14. Huang C, Xiong C, Kornfeld K. Measurements of age-related changes of physiological processes that predict lifespan of *caenorhabditis elegans*. Proc Natl Acad Sci U S A. 2004;101:8084–9.
15. Tu M, Yin C, Tatar M. Impaired ovarian ecdysone synthesis of *drosophila melanogaster* insulin receptor mutants. Aging Cell. 2002;1:158–60.
16. Castrillon DH, Miao L, Kollipara R, Horner JW, DePinho RA. Suppression of ovarian follicle activation in mice by the transcription factor Foxo3a. Science. 2003;301:215–8.
17. Burks DJ, de Mora JF, Schubert M, Withers DJ, Myers MG, Towery HH, et al. IRS-2 pathways integrate female reproduction and energy homeostasis. Nature. 2000;407:377.
18. Watkins WJ, Umbers AJ, Woad KJ, Harris SE, Winship IM, Gersak K, et al. Mutational screening of *FOXO3A* and *FOXO1A* in women with premature ovarian failure. Fertil Steril. 2006;86:1518–21.
19. Gallardo TD, John GB, Bradshaw K, Welt C, Reijo-Pera R, Vogt PH, et al. Sequence variation at the human FOXO3 locus: a study of premature ovarian failure and primary amenorrhea. Hum Reprod. 2007;23:216–21.
20. Das D, Arur S. Conserved insulin signaling in the regulation of oocyte growth, development, and maturation. Mol Reprod Dev. 2017;84:444–59.
21. Kalous J, Aleshkina D, Anger MA. Role of PI3K/Akt signaling in oocyte maturation and early embryo development. Cells. 2023;12:1830.
22. Kordowitzki P, Krajnik K, Skowronska A, Skowronski MT. Pleiotropic effects of IGF1 on the oocyte. Cells. 2022;11:1610.
23. Louhio H, Hovatta O, Sjöberg J, Tuuri T. The effects of insulin, and insulin-like growth factors I and II on human ovarian follicles in long-term culture. Mol Hum Reprod. 2000;6:694–8.
24. Duleba AJ, Spaczynski RZ, Olive DL, Behrman HR. Effects of insulin and insulin-like growth factors on proliferation of rat ovarian Theca-Interstitial cells. Biol Reprod. 1997;56:891–7.
25. Templeman NM, Luo S, Kaletsky R, Shi C, Ashraf J, Keyes W, et al. Insulin signaling regulates oocyte quality maintenance with age via cathepsin B activity. Curr Biol. 2018;28:753–60.
26. Lopez AL, Chen J, Joo H-J, Drake M, Shidate M, Kseib C, et al. DAF-2 and ERK couple nutrient availability to meiotic progression during *Caenorhabditis elegans* oogenesis. Dev Cell. 2013;27:227–40.
27. Michaelson D, Korta DZ, Capua Y, Hubbard EJ. A. Insulin signaling promotes germline proliferation in *C. elegans*. Development. 2010;137:671–80.
28. Rautela U, Sarkar GC, Chaudhary A, Chatterjee D, Rosh M, Arimbasseri AG, et al. Non-canonical role of somatic Cyclin D/CYD-1 in oogenesis and in maintenance of reproductive fidelity, dependent on the FOXO/DAF-16 activation state. PLoS Genet. 2024;20:e1011453.
29. Qin Z, Hubbard EJA, Non-Autonomous. DAF-16/FOXO activity antagonizes Age-Related loss of *C. elegans* germline Stem/Progenitor cells. Nat Commun. 2015;6:7107.
30. Ortiz MA, Noble D, Sorokin EP, Kimble J. A new dataset of spermatogenic vs. oogenic transcriptomes in the nematode *Caenorhabditis elegans*. G3 Genes|Genomes|Genetics. 2014;4:1765–72.
31. Wang X, Zhao Y, Wong K, Ehlers P, Kohara Y, Jones SJ, et al. Identification of genes expressed in the hermaphrodite germ line of *C. elegans* using SAGE. BMC Genomics. 2009;10:213.
32. Han M, Wei G, McManus CE, Hillier LW, Reinke V. Isolated C. *elegans* germ nuclei exhibit distinct genomic profiles of histone modification and gene expression. BMC Genomics. 2019;20:1–15.
33. Droujinine IA, Perrimon N. Defining the interorgan communication network: systemic coordination of organismal cellular processes under homeostasis and localized stress. Front Cell Infect Microbiol. 2013;3:82.
34. Ewels P, Magnusson M, Lundin S, Käller MMQC. Summarize analysis results for multiple tools and samples in a single report. Bioinformatics. 2016;32:3047–8.
35. Dobin A, Davis CA, Schlesinger F, Drenkow J, Zaleski C, Jha S, et al. STAR: ultrafast universal RNA-Seq aligner. Bioinformatics. 2013;29:15–21.
36. Liao Y, Smyth GK, Shi W. Featurecounts: an efficient general purpose program for assigning sequence reads to genomic features. Bioinformatics. 2014;30:923–30.
37. Love MI, Anders S, Kim V, Huber W. RNA-seq workflow: gene-level exploratory analysis and differential expression. F1000Res. 2015;4:1070.
38. Oliveros JCVENNY. An interactive tool for comparing lists with Venn diagrams. Httpbioinfogp Cnb Csic Estoolsvennyindex Html 2007.
39. Tang D, Chen M, Huang X, Zhang G, Zeng L, Zhang G, et al. SRplot: a free online platform for data visualization and graphing. PLoS One. 2023;18:e0294236.
40. Meiler A, Marchiano F, Haering M, Weitkunat M, Schnorrer F, Habermann BH. Annominer is a new web-tool to integrate epigenetics, transcription factor occupancy and transcriptomics data to predict transcriptional regulators. Sci Rep. 2021;11(1):15463.
41. Shannon P, Markiel A, Ozier O, Baliga NS, Wang JT, Ramage D, et al. Cytoscape: a software environment for integrated models of biomolecular interaction networks. Genome Res. 2003;13:2498–504.
42. Bindea G, Mlecnik B, Hackl H, Charoentong P, Tosolini M, Kirilovsky A, et al. ClueGO: a cytoscape plug-in to decipher functionally grouped gene ontology and pathway annotation networks. Bioinformatics. 2009;25:1091–3.
43. Jiao X, Sherman BT, Huang DW, Stephens R, Baseler MW, Lane HC, et al. DAVID-WS: a stateful web service to facilitate gene/protein list analysis. Bioinformatics. 2012;28:1805–6.

44. Puca AA, Chatgilialoglu C, Ferreri C. Lipid metabolism and diet: possible mechanisms of slow aging. Int J Biochem Cell Biol. 2008;40:324–33.
45. Mutlu AS, Duffy J, Wang MC. Lipid metabolism and lipid signals in aging and longevity. Dev Cell. 2021;56:1394–407.
46. Schroeder EA, Brunet A. Lipid profiles and signals for long life. Trends Endocrinol Metab. 2015;26:589–92.
47. Papsdorf K, Miklas JW, Hosseini A, Cabruja M, Morrow CS, Savini M, et al. Lipid droplets and peroxisomes are co-regulated to drive lifespan extension in response to mono-unsaturated fatty acids. Nat Cell Biol. 2023;25:672–84.
48. Folick A, Oakley HD, Yu Y, Armstrong EH, Kumari M, Sanor L, et al. Lysosomal signaling molecules regulate longevity in *Caenorhabditis elegans*. Science. 2015;347:83–6.
49. O'Rourke EJ, Kuballa P, Xavier R, Ruvkun G. ω-6 polyunsaturated fatty acids extend life span through the activation of autophagy. Genes Dev. 2013;27:429–40.
50. Luo S, Shaw WM, Ashraf J, Murphy CT. TGF-ß Sma/Mab signaling mutations uncouple reproductive aging from somatic aging. PLoS Genet. 2009;5:e1000789.
51. Tissenbaum HA, Ruvkun G. An insulin-like signaling pathway affects both longevity and reproduction in *Caenorhabditis elegans*. Genetics. 1998;148:703–17.
52. Lind MI, Ravindran S, Sekajova Z, Carlsson H, Hinas A, Maklakov AA. Experimentally reduced insulin/IGF-1 signaling in adulthood extends lifespan of parents and improves darwinian fitness of their offspring. Evol Lett. 2019;3:207–16.
53. Kaushik N, Rastogi S, Verma S, Pandey D, Halder A, Mukhopadhyay A, et al. Transcriptome analysis of insulin signaling-associated transcription factors in *C. elegans* reveal their genome-wide target genes specificity and complexity. Int J Mol Sci. 2021;22:12462.
54. Kumar N, Mukhopadhyay A. Using ChIP-Based approaches to characterize FOXO recruitment to its target promoters. FOXO transcription factors: methods and protocols. Springer; 2018. pp. 115–30.
55. Riedel CG, Dowen RH, Lourenco GF, Kirienko NV, Heimbucher T, West JA, et al. DAF-16 employs the chromatin remodeller SWI/SNF to promote stress resistance and longevity. Nat Cell Biol. 2013;15:491–501.
56. Antebi A. Inside insulin signaling, communication is key to long life. Sci Aging Knowl Environ. 2004;2004:pe25–pe25.
57. Yamawaki TM, Berman JR, Suchanek-Kavipurapu M, McCormick M, Gaglia MM, Lee S-J, et al. The somatic reproductive tissues of *C. elegans* promote longevity through steroid hormone signaling. PLoS Biol. 2010;8:e1000468.
58. Huang M, Hong M, Hou X, Zhu C, Chen D, Chen X, et al. H3K9me1/2 methylation limits the lifespan of *daf-2* mutants in *C. elegans*. Elife. 2022;11:e74812.
59. Guillermo AR, Chocian K, Gavriilidis G, Vandamme J, Salcini AE, Mellor J, et al. H3k27 modifiers regulate lifespan in *C. elegans* in a context-dependent manner. BMC Biol. 2021;19:59.
60. Savini M, Folick A, Lee Y-T, Jin F, Cuevas A, Tillman MC, et al. Lysosome lipid signalling from the periphery to neurons regulates longevity. Nat Cell Biol. 2022;24:906–16.
61. Lapierre LR, Gelino S, Meléndez A, Hansen M. Autophagy and lipid metabolism coordinately modulate life span in germline-less *C. elegans*. Curr Biol. 2011;21:1507–14.
62. Kumar N, Taneja KK, Kumar A, Nayar D, Taneja B, Aneja S, et al. Novel mutation in ATP-binding domain of ABCD1 gene in adrenoleucodystrophy. J Genet. 2010;89:473.
63. Qi W, Yan Y, Pfeifer D; Donner v. Gromoff, Wang E, Maier Y, Baumeister W. R. *C. elegans* DAF-16/FOXO Interacts with TGF-ß/BMP Signaling to Induce Germline Tumor Formation via mTORC1 Activation. *PLoS Genet.* 2017, *13*, e1006801.
64. He K, Zhou T, Shao J, Ren X, Zhao Z, Liu D. Dynamic regulation of genetic pathways and targets during aging in *Caenorhabditis elegans*. Aging. 2014;6:215.
65. Yamamoto KK, Savage-Dunn C. TGF-β pathways in aging and immunity: lessons from *Caenorhabditis elegans*. Front Genet. 2023;14:1220068.

Publisher's Note